Energy & Environmental Science

Accepted Manuscript

ROYAL SOCIETY OF CHEMISTRY

www.rsc.org/ees

Open circuit voltage of organic solar cells: An in-depth review

Naveen Elumalai[1]*Θ and Ashraf Uddin[1]*Θ

[1]School of Photovoltaic and Renewable Energy Engineering,

University of New South Wales, Sydney 2052, Australia

* Authors contributed equally to this work.

Θ Corresponding author – email: a.uddin@unsw.edu.au and n.elumalai@unsw.edu.au

Abstract

Organic solar cells (OSCs) have developed progressively in efficiency over the last two decades. Though it is promising, this technology is still far from realizing its full prospect. One of the most important parameter that determines the efficiency of OSCs is the open-circuit voltage (V_{OC}), which represents the maximum voltage a solar cell can provide to an external circuit. Light harvesting materials employed in OSCs have optical band gap of around 1.7 to 2.1 eV and yet the V_{OC} barely exceeds 1.0V, which is approximately just half of the photon's original energy. By contrast, in inorganic counterparts such as Si, CIGS and GaAs, the difference is only 0.3 to 0.45 eV between the material bandgap and V_{OC}. Hence, to achieve higher power conversion efficiencies (PCEs) in OSCs, a detailed understanding of the origins of V_{OC} and the associated energetic loss mechanisms is indispensable. The presented review takes an opportunity to elaborate various governing mechanisms and factors affecting the V_{OC} from a comprehensive yet insightful standpoint. This report also provides a concise synthesis of intricate interdependencies among the factors influencing V_{OC} and highlights potential research strategies to improve V_{OC}, rendering possible pathways to facilitate the viable commercialization of OSCs.

Keywords: Open Circuit Voltage, Organic Solar Cells, Density of States, Work function, Recombination, Interfaces.

Table of Contents

1. Introduction

Organic solar cells (OSCs) have shown their potential for the next generation photovoltaic devices. Device processing of OSCs is very simple compared to other existing photovoltaic technologies.[1] Organic semiconductors exhibit high absorption coefficients,[2] which allow very thin films to be used.[3, 4] The reduced manufacturing cost, coupled with reduction in material used, connotes that organic solar cells possess the potential to make a significant impact on the future PV market. The highest reported power conversion efficiency (PCE) for an OPV device is 12 %,[5] which is based on a small-molecule system, has already approached the benchmark what is deemed to be required for commercialisation. At present, OPV devices exhibiting the highest performance efficiency (PCE)[5] are based on the bulk heterojunction (BHJ) type, in which a blend composed of electron-donor material (small-molecule) and an electron-acceptor fullerene material are employed to form an active photovoltaic layer.[6-8] Moreover, the photovoltaic modules based on the organic solar cells (OSCs) has the lowest energy payback time (~ 0.4 years) compared to silicon (~2.4 years for c-Si) and CdTe (~ 0.7 years).[9] In order to push the efficiency limits beyond the existing boundaries, a basic understanding of the processes that control and limit the operation of solar cells is crucial and can serve as a guide for identification of new materials for high performance devices.[10] The power conversion efficiency (PCE) of an organic solar cell depends on the following photovoltaic parameters defined by the relation $PCE=J_{sc}V_{oc}FF/P_{in}$, where Jsc is the short circuit current, V_{OC} is the open-circuit voltage, FF is the fill factor, and Pin is the incident solar power.[11, 12] Having said that, one of the prominent limitations hindering the performance of OPVs to date is their low open circuit voltages (V_{OC}), which is typically less than half of the incident photon energy.[10] Light harvesting materials employed in OSCs have optical band gap of around 1.7 to 2.1 eV and yet the V_{OC} barely exceeds 1.0V, which is approximately just half of the photon's original energy. By contrast, in inorganic counterparts such as Si, CIGS and GaAs, the difference is only 0.3 to 0.45 eV between the material bandgap and V_{OC}.

Prominent and rigorous research is carried out targeting the open circuit voltage (V_{OC}) and efficiency (PCE) in organic solar cells with a consistent progress/development trend as depicted in Schematic 1. The trends clearly portray that the quest for higher V_{OC} and PCE is much greater in the last two years than any other years before - owing to the recent development in new materials, characterization techniques and processing conditions. Therefore, any research in organic solar cells aimed at improving efficiency (PCE) cannot overlook the open circuit voltage (V_{OC}) of the devices. Hence, to achieve higher power conversion efficiencies (PCEs) in OSCs, a detailed understanding of the origins of V_{OC} and the associated energetic loss mechanisms is indispensable.

Numerous studies have demonstrated that V_{OC} depends on the energy gap between the highest occupied molecular orbital (HOMO) level of the donor and the lowest unoccupied molecular orbital (LUMO) level of the acceptor of the BHJ, forming the basis for predicting the open circuit voltage in these devices.[13-19] Notably, Scharber et al.,[14] found an empirical relationship by analyzing V_{OC} across a wide range of materials combinations: $eV_{OC}=E_g-0.3eV$, where E_g is the donor-acceptor energy gap, and e is the elementary charge which. While this study was invaluable to engineering a new generation of donor polymers, it does not provide any significant physical insight as to the origins of V_{OC}. Till date; many models and empirical relationships were

formulated to address this debatable question: What causes the 0.3 eV losses, and how can it be reduced? Yet the conclusion for this query remains an open question till date. In this review, we take the opportunity to conglomerate the existing literature addressing this issue and elaborate various governing mechanisms and factors affecting the V_{OC} from a comprehensive yet insightful standpoint. This report also provides a concise synthesis of intricate interdependencies among the factors influencing V_{OC} and highlights potential research strategies to improve V_{OC}, rendering possible pathways to facilitate the viable commercialization of OSCs.

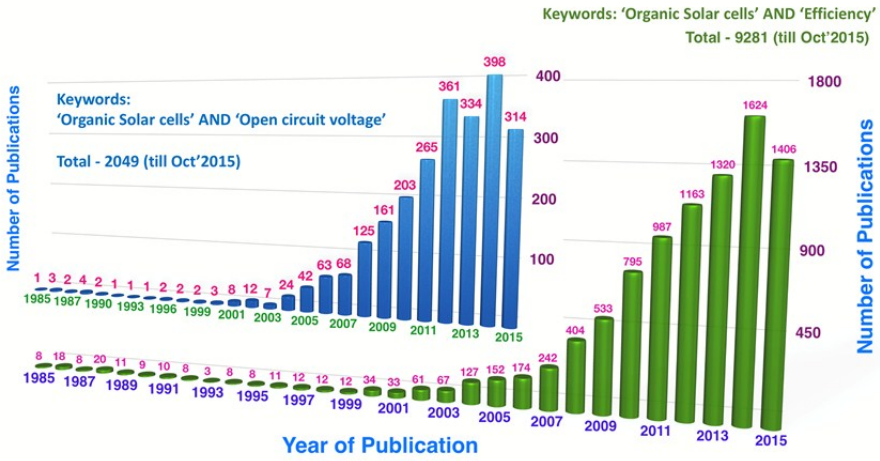

Schematic 1: (Inset) Graph showing the number of documents published w.r.t Open circuit voltage in organic solar cells. Graph details obtained from scopus with search filter as TITLE-ABS-KEY (**organic solar cells**) AND TITLE-ABS-KEY (**open circuit voltage**) from 1985 to 2015 with a total of 2049 documents. (Bottom) Graph showing the number of documents published w.r.t efficiency in organic solar cells. Graph details obtained from scopus with search filter as TITLE-ABS-KEY (**organic solar cells**) AND TITLE-ABS-KEY (**efficiency**) from 1985 to 2015 with a total of 9281 documents.

An overview of the mechanism/processes of the organic solar cell is discussed here before proceeding further: (1) light absorption and exciton generation (2) exciton dissociation into free carriers (holes and electrons) (3) the free carriers are transported to their respective electrodes via drift/diffusion phenomenon under the influence of the built-in potential and (4) collection of the free carriers at the electrodes and the current flows through the external load.[20-22] At the open-circuit condition under steady state illumination, the photogenerated free carriers will accumulate at the anode and cathode, constituting a potential difference, which cancels out the built-in potential. Under such condition, carrier generation and recombination exactly counterbalance each other; therefore, no net current exists at any point within the device. Now the system is said to be in a quasi-equilibrium state, and the potential difference between the two electrodes constitutes the open-circuit voltage (V_{OC}), which corresponds to the maximum voltage a solar cell can deliver to an external load.[11, 13, 22-24]

In general, V_{OC} originates due to the splitting of electron and hole quasi-Fermi energy levels actuated by light illumination:

$$V_{OC} = (1/q)(E_{Fn} - E_{Fp}) \quad (1)$$

where E_{Fn} and E_{Fp} are the electron and hole quasi-Fermi levels, respectively.[11, 23]

However, in practical conditions, this is not the case. Unlike crystalline inorganic semiconductors, which exhibit well-conceived hole and electron quasi fermi-levels, the organic semiconductors possess disorder induced gap tail states. Therefore, the distribution of photogenerated carriers in such gap tail states downshifts the electron quasi-Fermi level upshifts the hole quasi-Fermi level, thereby reducing the V_{OC} correspondingly as shown in Figure 1. Hence, direct determination of the electron and hole quasi-fermi level in bulk heterojunction organic solar cells is quite elusive.[25, 26] Moreover unique relationship exists between the V_{OC} and other influencing factors such as density of states or energetic disorder, charge transfer states, Donor-acceptor interface, microstructure, carrier density etc. which is of crucial importance in determining the V_{OC} of the devices. Apart from that, various other parameters that affect the V_{OC} of the organic (BHJ) solar cells are also discussed and elaborated in this review an over view of which is represented pictorially in Schematic 2.

Schematic 2: Factors influencing the open circuit voltage (V_{OC}) in organic solar cells. Each parameter influences the V_{OC} either directly or indirectly via interrelated dependencies among them.

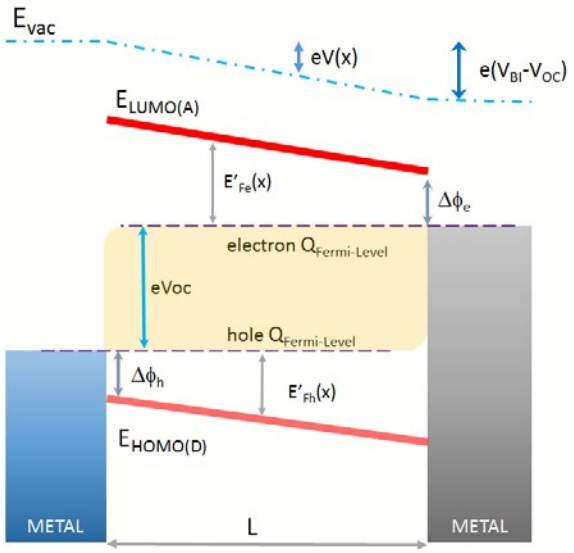

Figure 1. Energy-level diagram of an OPV device at open-circuit voltage. E_{vac} is the vacuum level (All energy intervals are defined as positive as shown in this diagram). $\Delta_{\varphi h}$ and $\Delta_{\varphi e}$ are the hole and electron injection barriers, respectively. V_{BI} is the difference in the contact work functions, $E_{Fh(x)}$ and $E_{Fe(x)}$ hole and electron quasi-Fermi potentials relative to their respective energy levels. Redrawn based on ref.[26]

2. Theory and origin of V_{OC}

A brief overview to the general solar cell equation is necessary for further understanding of the open circuit voltage (V_{OC}). The equivalent circuit of an ideal solar cell consists of a constant current source, a diode and an external load.[27]

Under light illumination a solar cell behaves like a current generator, delivering a photo-current density of J_{ph}. A small fraction of this current counteracts the diode junction current, and the remaining current flows to the load.[27]

According to Shockley's theory, the junction current density of the diode is expressed as:

$$J_d = J_0[\exp(qV/k_BT) - 1] \quad (2)$$

where k_B is the Boltzmann constant, T is the temperature and J_0 is the reverse saturation current density (typically in p-n junction solar cells it denotes the current density contributed by minority charge carriers, which is the total of the hole current in the n region and the electron current in the p region) and V is the output voltage.[27]

However, in the case of a practical solar cell, series resistance R_s and shunt resistance R_{sh} is non-negligeble.[3] R_s mainly constitutes the resistance of the bulk active layer, electrodes and also the interfacial contact resistance between the active layer and the electrodes. On the other hand, R_{sh} arises from numerous kinds of leakage

currents, which includes leakage current in the p–n junction, from the edge of the cell and by those induced by impurities in the cell, etc. Therefore, the actual current density J is a function of R_s and R_{sh} and can be written as:

$$J = \frac{R_{sh}}{R_{sh}+R_s}\left\{J_0\left[exp\left(\frac{q(V-JR_s)}{nk_BT}\right)-1\right]+\frac{V}{R_{sh}}\right\}-J_{ph} \quad (3)$$

At open circuit conditions, where $V = V_{OC}$, $J = 0$, and with the assumption that $R_{sh} \gg R_s$, V_{OC} can be expressed as:

$$V_{OC} = \frac{nk_BT}{q}\ln\left(\frac{J_{ph}}{J_0}+1\right) \quad (4)$$

It is noteworthy to mention that a new parameter called n (the ideality factor of the diode) in eqn (3) and (4).[11, 22, 27]

When $n = 1$, it signifies that the carrier recombination in the depletion region is zero (or negligible) and diffusion current is dominant in the device. On the other hand, when $n = 2$, it is vice versa. Under practical conditions, the device exhibits both recombination current and diffusion current, hence, the value of n normally ranges from 1 - 2. As the V_{OC} is directly proportional to n, the diode quality becomes poor when $n>2$.[27]

3. Factors influencing Open circuit voltage (V_{OC})

3.1 Reverse Saturation current (J_0)

Saturation current density or reverse saturation current (J_0) is one of the important parameter that determines the V_{OC} of the device. V_{OC} is inversely proportional to J_0 (eqn. 4) and hence lower the J_0, greater the V_{OC}. Therefore, the origin of saturation current density (J_0) is of significant interest in this regard. Potscavage *et al.* found that J_0 was exponentially dependent on temperature by using planar heterojunction devices based on pentacene/C_{60}.[28, 29] Their work concluded that J_0 arises from thermally activated carrier injection at the pentacene–C_{60} interface and the relationship is expressed as

$$J_0 = J_{00}exp\left(\frac{-\Phi_B}{k_BT}\right) \quad (5)$$

where J_{00} is a pre-factor determined by carrier generation and recombination rate, and Φ_B is the activation energy. Here the activation energy is defined as the offset between the HOMO of the donor and the LUMO of the acceptor (ΔE_{DA}) divided by a factor (larger than 1). The factor (>1) is introduced to account non-ideal effects such as formation of charge transfer states and vacuum level misalignments.[10, 28, 29]

Perez et al.[10] performed a similar work on OSCs with small molecules/C_{60} planar heterojunction and expanded the eqn. (5) as

$$J_0 = J_{00} exp\left(\frac{-\Delta E_{DA}}{2nk_BT}\right) \quad (6)$$

here the factor 2 denotes the parameters within thermal activation process i.e. considering that the two free carriers (holes and electrons) are simultaneously generated at the donor–acceptor interface. Hence, by substituting eqn (6) into (4), the relationship between V_{OC}, J_0 and ΔE_{DA} is elucidated as

$$V_{oc} = \frac{nkT}{q} ln\left(\frac{J_{sc}}{J_0}\right) + \frac{\Delta E_{DA}}{2q} \quad (7)$$

3.1.1 Relationship between V_{OC}, J_0 and ΔE_{DA}

The equation 7 denotes a linear dependence of V_{OC} on the interface energy gap (ΔE_{DA}) and a logarithmic dependence on J_{SC} and J_0. The short circuit current J_{SC} is directly proportional to the illumination intensity, which is experimentally, observed in both bulk and planar heterojunction OSCs.[18, 30-34] A linear correlation of V_{OC} to ΔE_{DA} has been reported previously for several materials systems and ΔE_{DA} provides the activation energy required for charge separation at the donor acceptor (D/A) interface.[14, 16, 32] Therefore, it is clear that in order to achieve maximum V_{OC} for a given D/A pair, J_0 must be minimized. As convincing as it could be, these expressions as discussed above are concluded from experiments based on planar heterojunctions and hence its complete applicability on BHJ solar cells is still questionable. In order to close this gap, Vandewal et. al. deduced the relationship between V_{OC} and J_0 in BHJs using the detailed balance from electroluminescence and photocurrent quantum efficiencies rather than using dark current.[23] Here, the ideality factor m is nearly always found to be greater than 1 which is also corroborated from other similar reports in OSCs.[10, 15, 23, 32] Therefore, V_{OC} in OPVs is highly influenced by recombination and its related mechanisms, which would be discussed in detail in the following sections.

3.2 Recombination

The power conversion efficiency (PCE) of a solar cell is defined by the relation $PCE=J_{sc}V_{oc}FF/P_{in}$, where J_{sc} is the short circuit current, V_{OC} is the open-circuit voltage, FF is the fill factor, and P_{in} is the incident solar power.[11, 12, 35-38] As the carrier recombination results in loss of photogenerated charge carriers, gaining a discernment of the mechanisms governing the recombination is vital for enhancing the solar cell performance and V_{OC}. Generally, V_{OC} is related to interface energy gap (ΔE_{DA}) or effective band gap $E_g=[E_{LUMO(A)}–E_{HOMO(D)}]$, but it hinges on a number of parameters, e.g. illumination intensity, temperature, exciton generation rate, mobility of charge carrier, charge carrier lifetime and recombination rates. In addition, better photovoltaic efficiency of molecular heterojunctions requires Ohmic contacts and meticulous tuning of the electron-transfer rates at the heterojunction.[39-41]

Therefore, it is essential to study the recombination processes for understanding of origin and nature of V_{OC}. The recombination process is limited by the recombination rate *R*. In order to quantitate the recombination rate *R* in OSCs, it is necessary to identity the type of recombination existing in the device i.e. whether the recombination - is monomolecular, or bimolecular, or an amalgamation of the two. In case of monomolecular recombination, carriers recombine through a recombination centre (or a trap) and whereas in the case of bimolecular recombination; the non-geminate carriers (holes and electrons) recombine.

A latest study has pointed out that the recombination mechanism can switch from monomolecular at short circuit condition to bimolecular at open circuit condition.[42]

Under short circuit conditions, the main recombination is predominantly monomolecular (trap-induced) because the electrons and holes are spatially alienated and swept out rapidly by the built-in potential. On the other hand, at open circuit condition (V_{OC}), bimolecular recombination is significantly increased as the built-in potential is cancelled out and photo-generated carriers linger/accumulate within the device.[43, 44] Under practical working conditions, the output photo-voltage can vary from zero to V_{OC} depending on the resistance of the external load and the corresponding recombination thereby progressively shifts from monomolecular recombination to monomolecular/bimolecular co-dominated regime, and then finally to bimolecular recombination.

3.2.2 Recombination Rate at Open circuit voltage

At open circuit condition, the photogenerated current J=dJ/dx=0 i.e., the net current and the current flux are both equal to zero. Considering both monomolecular (interfacial recombination mediated by traps) together with bimolecular recombination at steady state, the following expression is formulated[42]

$$\frac{\partial n_{e,trap}}{\partial t} = \left(R_{e,trap} - G_{e,trap}\right) - \left(R_{h,trap} - G_{h,trap}\right) = 0 \qquad (8)$$

where, n_e is the density of electrons at the LUMO level of fullerene (acceptor) and n_h is the density of holes at the HOMO level of polymer (donor), $G=G_e=G_h$ is the exciton (electron-hole pairs) generation rate as a function of photo absorption upon illumination, $G_{e,trap}$ is the rate at which trapped electrons are thermally ejected from a trap into the LUMO of fullerene, $G_{h,trap}$ is the rate at which trapped holes are ejected from traps into the HOMO of polymer, R_b is the bimolecular recombination rate, $R_{e,trap}$ is the rate at which electrons fall into (interfacial) traps from the LUMO of fullerene and $R_{h,trap}$ is the rate at which holes are lost to traps.[42]

Assuming that all excited electron-hole pairs diffuse to the polymer-fullerene interface and dissociate into electrons at LUMO of acceptor (fullerene) and holes at the HOMO of donor (polymer) and the traps are situated predominantly at the interface of polymer and fullerene domains, the recombination rate (R) at open-circuit voltage can be written as

$$R\,(V_{oc}) = G = \frac{n_{oc}}{\tau_r} + \gamma n_{oc}^2 \qquad (9)$$

where τ_r is the monomolecular recombination lifetime, γ is the bimolecular recombination coefficient and n_{oc} is the electron (or hole) density inside the device at open circuit conditions.[42] Moreover, Street et al. has reported that near short circuit condition, bimolecular recombination is inhibited relative to monomolecular (trap-induced) recombination because the number of electrons or holes present per domain is <1 (and often zero), where the domain size is of the order 10^{-17} cm^{-3}.[42, 45]

The recombination mechanism controls the degree to which the incident light intensity influences the V_{OC}. At open circuit conditions upon illumination, the voltage applied matches the difference between the quasi-Fermi levels within the polymer and fullerene phase separated domains/regime. Based on this observation, the following expression for the open-circuit voltage is obtained:[42]

$$V_{oc} = \frac{1}{e}\left(E_{LUMO}^{Fullerene} - E_{HOMO}^{Polymer} - \Delta\right) - \frac{kT}{e}\ln\left(\frac{n_e n_h}{N_c^2}\right) \quad (10)$$

where n_e is termed as the electron density in the fullerene domains and n_h is termed as the hole density in the polymer domains at open circuit conditions, and N_c is the density of states (DOS) at the conduction band edge of the polymer and fullerene. The energy shift, Δ, in Eq. 10 arises from disorder within the phase separated polymer and fullerene domains. Therefore, the generally expected value of V_{OC} as a function of the difference in E_{ALUMO} and E_{DHOMO} (i.e. $V_{OC} \approx E_{ALUMO} - E_{DHOMO}$) is obtained only at T=0 K following the Eq. 10. The rationality of the initial term in Eq. 10 has been tested for numerous polymer: fullerene BHJ systems but resolved with a drop of 0.3 V.[13] The missing 0.3 V is expected to arise due to the fundamental statistics of Fermions. At finite temperature T, the quasi-Fermi levels transgress away from E_{ALUMO} and E_{DHOMO} respectively i.e. into the gap above the polymer HOMO and below the fullerene LUMO and this anomalous distribution is estimated to be one of the origins of the "missing 0.3 V."[42] In spite of such attempts to understand the origins of the losses in V_{OC}, the open circuit voltage seldom exceeds 1.0 V in OSCs materials, which commonly have optical gaps between 1.7 and 2.1 eV.[46, 47] The difference of 0.7 to 1.1 eV between the optical gap and $qV_{oc,}$ is approximately half of the photon's original energy leaving a cue of how it's important to close this gap to push the PCE closer to maximum achievable limits.[47] Therefore, in-depth understanding of V_{OC} and its influencing parameters is indispensable for designing better devices to achieve higher efficiencies.

3.3 Temperature and illumination intensity

Open circuit voltage in bulk heterojunction OSCs is found to decrease linearly with increase in temperature and it is widely attributed to the temperature dependent mobility.[31, 48-51] Furthermore, experimental results using several BHJ configurations and flexible roll-to-roll coated modules[52] found that V_{OC} linearly decreases with temperature exhibiting a temperature coefficient of order of 1 mV K^{-1} around room-temperature. Sarah et al. studied the temperature dependence of V_{OC} in PCDTBT:PC_{71}BM based BHJ solar cells under various illumination intensity.[42] They demonstrated that by fitting the experimental data using the equation (7) and

extrapolating them to T=0K, a convincing prediction emerged in which that the dashed lines converge at the maximum interfacial band offset V_{OC} of 1.25V (see figure 2) equal to 1/e ($E_{ALUMO}-E_{DHOMO}-\Delta$) at T=0K.

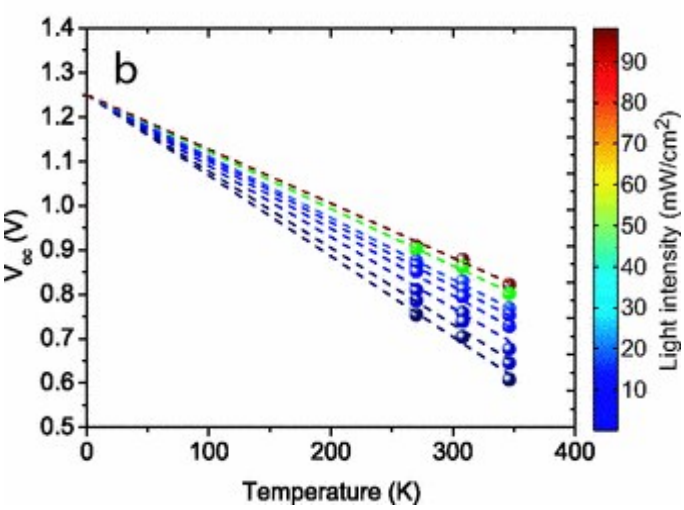

Figure 2. Linear dependence of V_{OC} with temperature at various light intensities. The dashed lines fit well to the data and predict an interfacial band offset $V_{OC}=e(E_{FullereneLUMO}-E_{PolymerHOMO}-\Delta)=1.25V$. Reprinted with permission from ref.[42] Copyright 2010 American Physical Society.

However, experiments involving actual temperature closer to 120K have revealed that the linear dependence of V_{OC} on temperature deviates from its trend.[32, 53-55] Rand *et al.* observed V_{OC} saturation at lower temperatures (around 150K) in numerous small molecular heterojunction solar cells with bilayer configuration[32] (Fig. 3a). V_{OC} saturation is ascribed to the decrease in J_{ph} because of the decreased electron transfer rate from donor (D) to acceptor (A). The decrease of J_{ph} is also partly attributed to reduced mobility at low temperatures, at which carrier mobility is limited by localized states.[56] Studies from Garcia et al.[57] and Thakur et al.[58] has described the V_{OC} saturation at low temperature in bulk heterojunction OSCs and rationalized the deviation from linear trend attributing to the Fermi level displacement with temperature and occupancy of the density-of-states. They observed that when T is greater than 200 K, the V_{OC} is predominantly influenced by recombination and a linear dependence of V_{OC} on T is observed. When T is less than 200 K, the tail states disorder (DOS occupancy) is the major cause of loss, causing the V_{OC} to deviate from the linear fit. Thus, the phenomenon of V_{OC} saturation could be employed to estimate the degree of disorder in OSCs.[58, 59]

Recently, Gao et al.[53] found similar deviation in V_{OC} at low temperature in BHJ devices employing polymer:fullerene and polymer:polymer blends (see figure 3). They argued that a strong relation exists between the carrier separation and V_{OC}, which leads to anomalous decrease of V_{OC} at low temperature and corroborates the critical role of charge delocalization in charge separation and its influence on V_{OC}. They found that the reason for the variation in the transition temperature (where V_{OC} starts to saturate or decrease) is due to reduced charge separation owing to decrease in electron-hole distance in charge transfer (CT states) at low T.

Moreover, the temperature-dependent analyses performed on BHJ solar cells suggest that the quasi-Fermi levels are not effectively pinned at the interfacial band gap. Variations in the quasi-Fermi levels caused by the thermal alterations are in fact the main reason behind the voltage difference observed between the interfacial band gap and the V_{OC} (evaluated at room temperature). Moreover, localization of the photogenerated carriers at low

temperatures due to reduced mobility would cause a nonlinear reduction in the current and the V_{OC}, therefore making the process of quantifying the complete interfacial gap at low temperatures quite difficult under practical conditions though it appears to be theoretically probable. Adding to the argument, the quasi-Fermi levels variations as a function of temperature in the polymer and fullerene domains is found to be one of the reasons for the "missing 0.3 V" in V_{OC} as observed by Brabec *et al.*[13, 42]

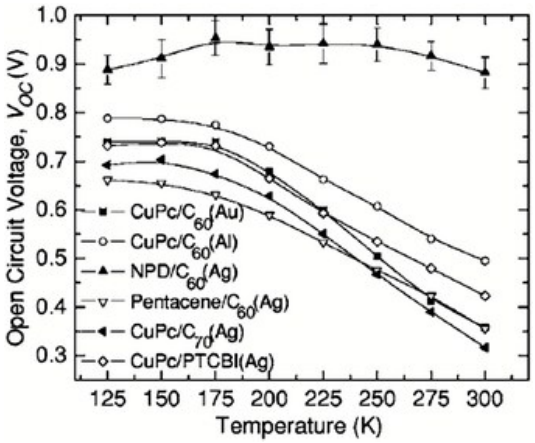

Figure 3a. V_{OC} versus Temperature (T) for various donor–acceptor heterojunctions. The metal in parentheses in the legend point to the cathode material used for that device. Reprinted with permission from ref.[32] Copyright 2007 American Physical Society

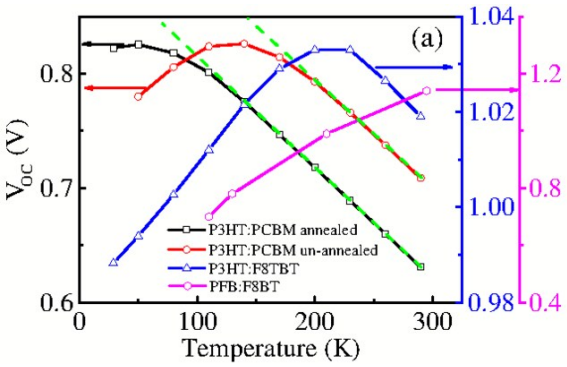

Figure 3b. Temperature-dependent V_{OC} for devices with BHJ blend P3HT:PC60BM, P3HT:F8TBT, and PFB:F8BT. At low T, the V_{OC}-T plot deviates from the linear relation (dashed line), starting to saturate and even decrease. Reprinted with permission from ref.[53] Copyright 2015 American Physical Society

3.3.1 Light Intensity

The net current is zero at open-circuit conditions (V_{OC}), i.e. all the photogenerated carriers recombine within the device. Thus, recombination analysis at/near open circuit is particularly susceptible to the particulars of the recombination mechanism. The open-circuit voltage varies logarithmically with illumination intensity as shown in fig. 4a and that all the curves of δV_{oc} vs ln(I) for polymer:fullerene BHJ solar cells have the same slope,(k_BT/e).The fig. 4b also shows the trend of a-Si solar cell (red line), with $\delta Voc \sim 1.7$ (k_BT/e) and that of single crystal silicon cells.[42] By comparison (fig. 4b), it can be inferred that the well-defined quasi fermi levels in single crystal silicon solar cells exhibit higher slope relative to that of the BHJ OSCs. The revelation substantiates that the density of states distribution (Gaussian for OSCs and well defined for crystalline Si cells) plays a crucial role in defining the V_{OC} as a function of light intensity. Figure 4b shows the universal/general trend of δV_{oc} in OSCs and the inset depicting that the density of states (DOS) in the band "tails" and the intensity-dependent quasi-Fermi energies (at T=0 K – refer dotted lines) as the tails are occupied by photoexcited electrons (in the fullerene section) and holes (in the polymer section). At finite temperatures, the quasi-Fermi energies move into the gap thereby reducing the V_{OC}.

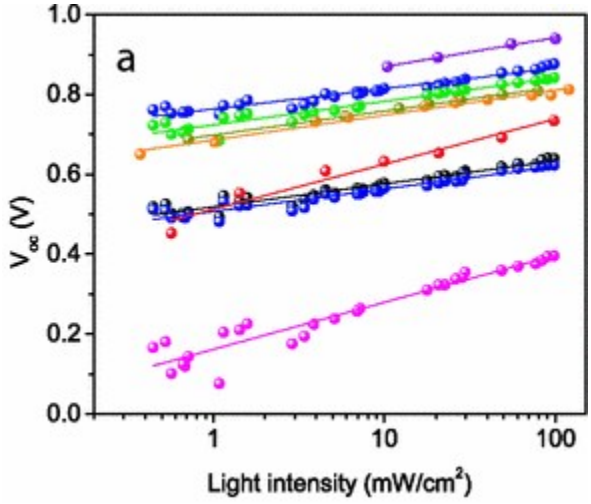

Figure 4 (Color) (a) Open-circuit voltage as a function of incident light intensity for various BHJ blend systems; OC1C10: PPV: DPM-10 (purple) (Ref. 21), PCDTBT Mw=100 kDa:PC71BM (royal blue), PCDTBT Mw=58 kDa: PC71BM (green), BEH: PPV: PC60BM (tan) (Ref. 22), MDMO: PPV: PC60BM (yellow) (Ref. 23), P3HT: PC60BM (black), KP: PCBM (dark blue), amorphous silicon (red), and single-crystal silicon (pink). Reprinted with permission from ref.[42] Copyright 2010 American Physical Society

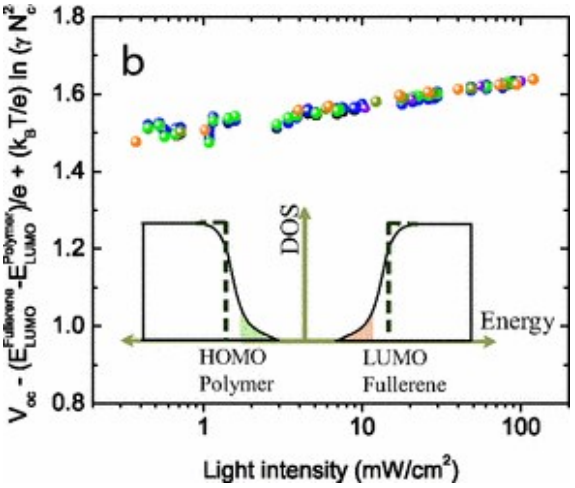

Figure 4(b) Universal curve showing slope of δVoc. V_{OC} trend under varying illumination intensity is directly correlated to DOS. Reprinted with permission from ref.[42] Copyright 2010 American Physical Society

Sarah et al.[42] has also demonstrated that observed that V_{OC} under higher illumination intensities is converged at 0 K (see figure 2), which provides the evidence about maximum achievable V_{OC} in a particular donor–acceptor blend. Furthermore, Thakur et al.[58] studied the recombination processes in P3HT:PCBM based BHJ OSCs; as a function of light and temperature, by using transient open-circuit voltage decay (TOCVD) measurements. They found that at low $V_{OC,}$ carrier lifetime exhibits a constant value ~500 μs, which is inferred in terms of a monomolecular recombination regime as shown in Fig. 5a. At higher $V_{OC,}$ carrier lifetime drops rapidly following the bimolecular relaxation law. Additionally, a changeover from bimolecular to monomolecular recombination mechanisms for high and low V_{OC} is noticed at respective conditions.

Figure 5b. shows the experimental trends of V_{OC} as a function of temperature under different light intensities for P3HT:PCBM based BHJ devices. It clearly indicates that the convergence only happens under high illumination intensities. Though the curves of V_{OC} versus temperature are still linearly dependent on temperature as expected from eqn. (7); they do not converge at 0 K under lower intensities of illumination. The reason for this variation is as discussed earlier - under illumination, V_{OC} is associated to the splitting of quasi Fermi levels is contingent on the charge carrier densities in the fullerene (LUMO) and polymer (HOMO) density-of-states (DOS).[60, 61] Further in-depth discussion on the influence of DOS on V_{OC} is elaborated in its respective section.

3.4 Carrier density

The recombination rate of charge carriers is reliant on the carrier density in BHJ OSCs, which directly influences the V_{OC}. The recombination rate is higher when the carrier density is higher which in turn is contingent on the voltage. As the forward bias voltage is applied, it counteracts the in-built photovoltage causing

the carriers to stagnate within the device and leading to increase in carrier density. As discussed earlier, the V_{OC} is the voltage at which the photo-generation rate and the recombination rate exactly cancels out each other. Maurano *et al.*,[40] quantified carrier densities and recombination rates at open-circuit conditions under different light intensities. In their report, they parameterized the recombination rates by employing empirical power-law dependence while the carrier density was parameterized by using an empirical exponential dependence on voltage. Combining these two factors, a logarithmic dependence of V_{OC} as a function of light intensity was observed, which is in agreement with experiments.[40]

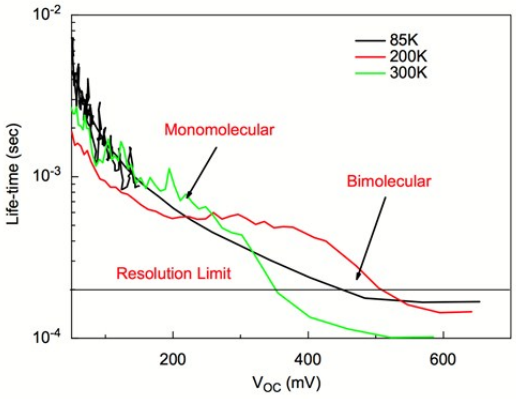

Figure 5a. (Left) Effective time constants (τ_{eff}) versus V_{OC} at different *T*. Reprinted with permission from ref.[58] Copyright 2011 Elsevier

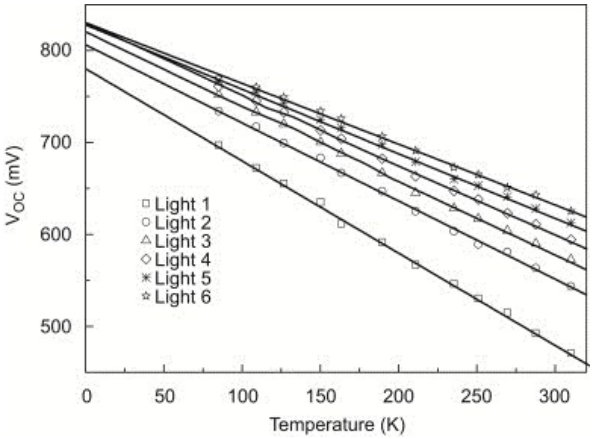

Figure 5b. (right) Extrapolated plot of V_{OC} (mV) at different illumination intensity versus temperature (K) in P3HT: PCBM based BHJ devices. Reprinted with permission from ref.[58] Copyright 2011 Elsevier

While this general approach is able to define the behaviour of numerous material systems in terms of V_{OC}, it offers diminutive physical insight into the origins of dissimilarities in V_{OC} between materials. On the other hand, the ideal BHJ diode model postulated by Koster et al.[62] (see eqn. 12) predicts V_{OC} in terms of physical parameters, such as the donor-acceptor energy gap and recombination rate coefficient as expressed in eqn.12[62]

$$V_{oc} = \frac{E_{gap}}{q} - \frac{kT}{q}\ln\left(\frac{(1-P)\gamma N_c^2}{PG}\right) \qquad (11)$$

Here E_{gap} is the effective band gap ($E_{FullereneLUMO}$–$E_{PolymerHOMO}$), Nc is the effective density of states (DOS), P is the dissociation probability of a bound electron–hole pair into free charge carriers, G is the generation rate of bound electron-hole pairs, γ is the Langevin recombination constant. The product PG then represents the generation rate of free charge carriers.[62] While discerning, this model fails to envisage the exact dependence of V_{OC} on light intensity for the majority of real devices. It is noteworthy to mention that the investigation of the temperature dependence of V_{OC} of polymer: fullerene solar cells (using equation (12)) are intensely complex due to the nonexistence of a sharply defined band gap. In simple, the equation (12) does not take into the account of the existence of energetic disorder in both donor and acceptor materials, infact their HOMO and LUMO levels display a Gaussian broadening σ of typically at-least 0.1 eV.[56, 62] Therefore, since the exact

distribution of energy levels is not quantified, the uncertainty in E_{gap} is of the similar order of magnitude as the variation of V_{OC} with temperature, thereby prohibiting an exact quantitative analysis. As a result, V_{OC} of most of the real devices are not compliant with the intensity dependence predicted by this ideal model, and variation in the density of states or energetic disorder should be considered in developing a suitable general model to explain the variation in V_{OC}, which is discussed in the next section.

3.5 Density of States (DOS) and energetic disorder

Although the recombination losses predominantly occurs at the donor/acceptor interface, the role of energetic disorder cannot be disregarded, which is significantly inherent to organic layers.[60, 63] Energetic disorder in the organic semiconductors, characterized by the scattering of the electronic density of states (DOS) of the donor and acceptor materials constituting the active layer, plays an important part in governing open-circuit voltage V_{OC}, which is found to scale with $\Delta E_{D.}$[14, 44, 51] However, the donor HOMO and acceptor LUMO levels are generally determined from cyclic voltammetry of the respective materials in solution form, or sometimes in combination with absorption experiments,[64, 65] which cannot precisely account for the fine details about the energetic disorder involved in the organic semiconductors, consequently the deviation of V_{OC} values from E_g is left unexplained.[57, 64] Moreover, it was also found that the electronic states in the fullerene exhibit broad energy dispersion. The shape of the DOS distribution has the Gaussian form, as commonly anticipated in organic materials affected by structural or chemical defects.[21, 66] Having said that, the energy states at the higher level in the fullerene are typically not accessible since the recombination kinetics severely limits the occupation preferably to the DOS tail states. In general, the existence of energetic disorder in the materials forming the solar cell has a significant influence on the photo-physics/processes that determines the photovoltaic properties of the device. Moreover, in organic blends where the phase segregation between the D/A materials are on the nanometre scale, energetic disorder eliminates any coherence effects, and the charge carriers are mostly localized.[66] Garcia et al.[57, 60] have reported that the V_{OC} limit is caused by recombination through tail states in BHJ (polymer-fullerene) solar cells. They demonstrated that the energetic disorder of the electronic density-of-states (DOS) of acceptor and donor materials decreases the fermi-level splitting of the electron and hole in bulk heterojunction solar cells, by confining the accumulation of carriers into the tails of the DOS. Garcia et al.[57, 60] proposed a model to predict the achievable V_{OC} values by incorporating the density of states (DOS) distributions of both donor HOMO and acceptor LUMO manifolds. In their work, the energetic disorder (prevalent for organic conductors) is modelled by means of Gaussian DOS with mean energy E_{LUMO} and width σ_n for the acceptor fullerene (and E_{HOMO} and width σ_p for the donor polymer).[21] A broad distribution of the Gaussian DOS is considered because $\sigma \approx 2k_BT - 4k_BT$ (being k_BT the thermal energy) which is depicted in Figure 6a.[60]

Under steady-state conditions, thermalization of the photogenerated carriers (primarily distributed along DOS shape) into the Gaussian tail states occurs, following a Boltzmann statistics with an average, equilibration energy $E_{mn}=\sigma 2n/k_BT$ below the LUMO mean. Here the mean energy level of the charge carriers is positioned above the Fermi level, i.e., $E_{Fn}<E_{mn}$.[21] Similarly for holes, the equilibration energy $E_{mp}=\sigma 2p/k_BT$ is above the

HOMO mean.[60] Using the rational discussed above, Garcia et al.[57] derived an expression for the DOS for holes and electrons in disordered organic conductors exhibiting a Gaussian distribution, $g_{h/e}(E)$ as

$$g_{h/e}(E) = \frac{N_{h/e}}{\sigma\sqrt{2\pi}} \exp\left[-\frac{\left(\pm E \mp E_{HOMO,D/LUMO,A}\right)^2}{2\sigma^2}\right] \quad (12)$$

Here N defines the total DOS (hole or electron states) with mean energy E_0 and width σ (width of the Gaussian DOS) quantifies the energetic disorder in the Gaussian distribution. Hence, the distribution of the DOS is broad if $\sigma > k_B T$ (see figure 6a). Moreover, in can be inferred from Figure 6b that the electron in a localized state of the fullerene recombines with a hole in the polymer is indicated by an arrow (A) and similarly an electron undergo recombination via hopping to nearby unoccupied localized states represented by arrow (B). Blakesley et al.[26] has simulated the influence of energetic disorder on V_{OC}, and observed that as the disorder (σ) increases, V_{OC} drops as expected as shown in Figure 7a and 7b. Moreover, both J_{SC} and FF also drop along with V_{OC}, the reason is attributed to the disorder induced carrier traps decreasing the carrier mobility. Therefore, energetic disorder plays an important role in decreasing the attainable open-circuit photovoltage in BHJ OSCs.

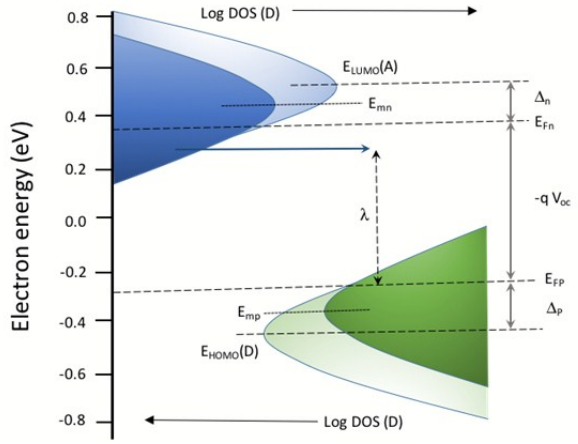

Figure 6a Diagram showing the acceptor HOMO (donor LUMO) Gaussian DOS (line), and LUMO occupied (HOMO unoccupied) states (filled area) by thermalized carriers resulting from the kinetic balance between photogeneration and recombination fluxes. The recombination event (horizontal solid arrow) is indicated for a given value of the reorganization energy λ. The origin of the photovoltage is marked as $-qVoc=E_{Fn}-E_{Fp}$, and the offset energy $\Delta=\Delta n+\Delta p$. Photogenerated carriers accumulate around E_{mn} and E_{mp}. Redrawn based on ref.[60]

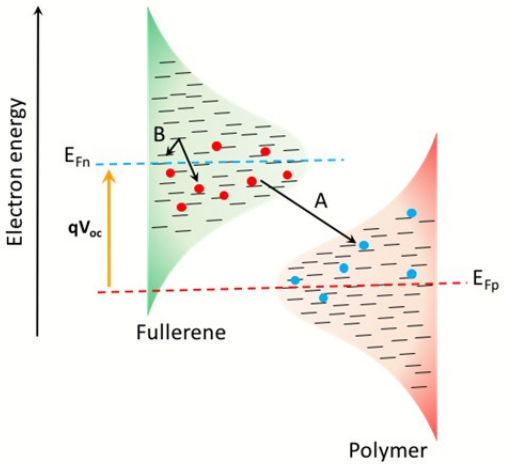

Figure 6b. Energy scheme depicting the Gaussian density of states (DOS) in both the polymer and fullerene materials. Thermalized electrons in the fullerene and thermalized holes in the polymer are located mostly, in the lower and upper tails of the DOS, respectively. An arrow (A) indicates recombination of an electron in a localized state in the fullerene with a hole in the polymer. An electron can also recombine (or separated from interface) via hopping to nearby vacant localized states (B). Redrawn based on ref.[57]

Moreover, the electronic states of molecules in organic semiconductors films (during device fabrication) are subject to random energetic variations due to the factors such as variations in conjugation length, interactions with neighbouring conjugated molecules, rotations and kinking of polymer chains, impurities and dipoles from residual solvent molecules, etc. It is noteworthy to mention that this disorder is not only intrinsic to the

molecular structure, but it is also a property of the solid film, which is strongly dependent on film preparation.[63, 67-70] In addition, several studies have employed the concept of energetic disorder to elucidate numerous phenomena in organic semiconductors, such as temperature, electric field, and carrier density–dependent charge-carrier mobility,[21, 71-73] reduced charge injection barriers, and increased band bending at the interfaces.[74, 75] Moreover, the intrinsic dopant levels are characteristically lower in organic semiconductors, such that the tail states are not totally occupied in OSCs operation. Hence, the relaxation of carriers into deep tail states has to be considered as a noteworthy process in determining the V_{OC} and hence the device performance.

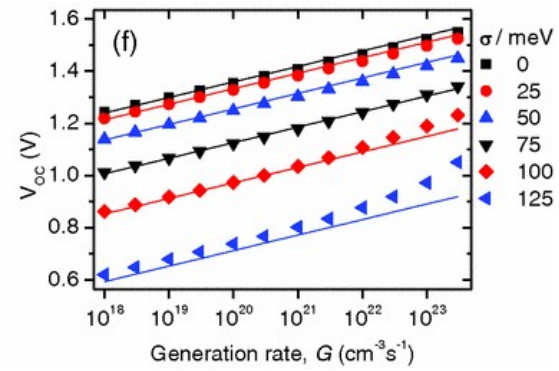

Figure 7a V_{OC} vs. intensity with varying disorder and field-dependent generation and recombination. Reprinted with permission from ref.[26] Copyright 2011 American Physical Society

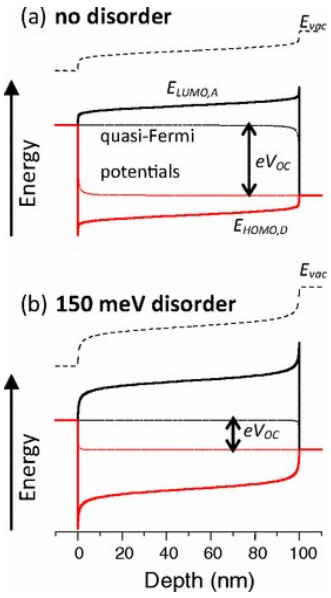

Figure 7b Simulated energy diagrams in open-circuit conditions with G = 10^{20} $cm^{-3}s^{-1}$ and (a) no disorder. (b) σ = 150 meV Gaussian disorder. Reprinted with permission from ref.[26] Copyright 2011 American Physical Society

In line with the discussion, Lange et al.[25] developed a measurement technique combining Bias Amplified Charge Extraction (BACE) with Kelvin Probe (KP) measurements to extract information on the relevant energetics in the blend. They studied the variation of V_{OC} with respect to steady state carrier density in polymer: fullerene blends using (BACE) measurements and pointed out that the Gaussian type disorder in the blend plays a significant role in determining the charge carrier density as well as the V_{OC} of the device. Figure 8 displays that the extrapolation of the BACE data to a carrier density of 10^{15} cm^{-3} yield a V_{OC} of 520 mV, which corresponds quite well to the quasi fermi level-splitting of about 470 meV as deduced from the Kelvin-probe experiments. Lange et al. also showed that the dependence of V_{OC} on blend composition and thermal dependency to be largely determined by variations of the fullerene LUMO energetics.[25]

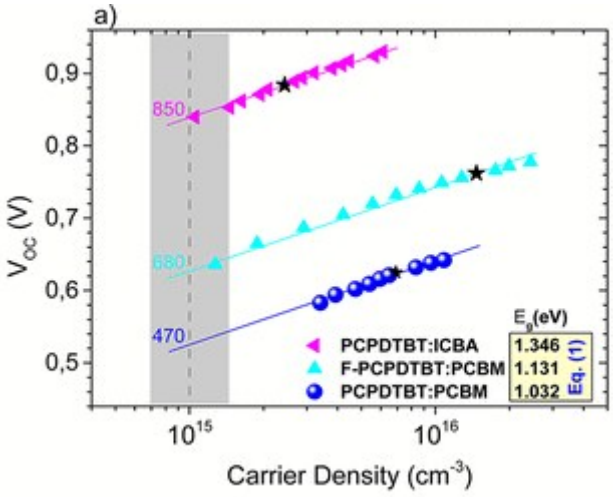

Figure 8 V_{OC} versus carrier densities n for PCPDTBT:PCBM, F-PCPDTBT:PCBM and PCPDTBT:ICBA as measured by BACE. The star shows V_{OC} according to AM 1.5G illumination. Reprinted with permission from ref. [25] Copyright 2013 American Chemical Society.

3.6 Defect states and Crystallinity

Defect states and crystallinity can be deliberated as some of the additional sub-parameters that affects the energetics as discussed in the previous section. Lange et al. showed that a decisive factor of open-circuit voltage is the magnitude of energy distribution of intermediate electronic states (IDOS) beneath the LUMO level of the acceptor. They demonstrated that the less crystalline fullerenes (DPM_6) allow for a higher rise of the fermi level via reduction of the available number of electronic states as shown in Figure 9b.[57] Likewise, the influence of composition and preparation conditions on the defect states and crystallinity was also observed in P3HT:$PC_{70}BM$ based devices as depicted in Figure 9a.[76] Though reasonable upward shifts of the P3HT HOMO were observed, depending on P3HT crystallinity, the dependence of V_{OC} on blend composition is predominantly determined by the variation in the PCBM LUMO energy.[76] It was found that the device processing that enables an increased crystallinity of the film is advantageous for the device performance as it reduces the defect density (energy disorder) that finally increases the maximum achievable V_{OC}, despite the upward shift of the polymer HOMO manifold.

3.7 Work function of electrodes

The relationship between open-circuit voltage (V_{OC}) and the work function (φ) is still a matter of debate. In general, when the contact fermi level lies close to either $E_{HOMO,D}$ or $E_{LUMO,A}$, V_{OC} is independent of the contact work function. Between these parameters, there is a slope of 1 which is fairly consistent with experimental observations.[13, 18] For Ohmic contact, under thermal equilibrium, the Fermi level of the cathode will be levelled and pinned to the LUMO level of the acceptor.[73] The same phenomena apply to the donor and anode, where the Fermi level of the anode is pinned to the HOMO level of the donor when an Ohmic contact is established. As previously observed, disorder reduces V_{OC} and the disorder tends to be lower when both contacts are Ohmic. It

is noteworthy to mention that the effect of disorder is nearly half even when only one of the contacts is pinned.[74] It was recently demonstrated that the band bending governs the limits of Fermi-level pinning in polymer films of more than about 10 nm thickness.[74] These results are reminiscent of a strong association between band bending and V_{OC}. If the energetic barrier for holes transfer between the anode and the donor is high, the contact is considered non-Ohmic. Under non-Ohmic contact, substantial surface recombination at the active layer–cathode interface occurs, whereas under Ohmic contact, such surface recombination is significantly suppressed and can hence be ignored**.** If both contacts are non-Ohmic, V_{OC} is then determined by the variation in the work functions of the two electrodes, as forecasted by the MIM model (Metal–Insulator–Metal) as shown in Figure 10 (represented as V_{OC} 2).[44]

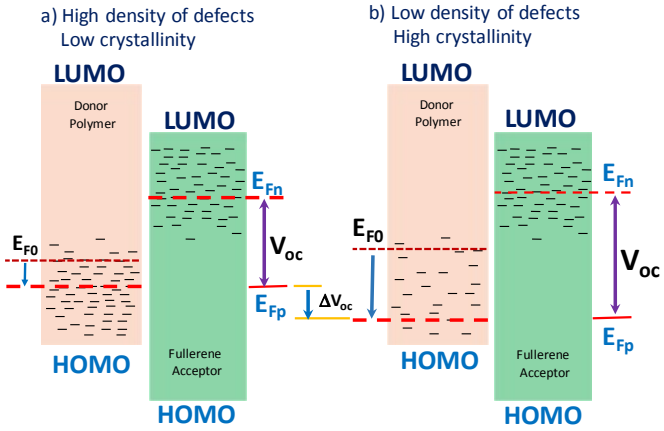

Figure 9a Energy diagram of the polymer:fullerene blend under illumination indicating the electrically active states in the band gap of both materials. The donor HOMO level is displaced depending on the polymer crystallinity. The position of the equilibrium (dark) Fermi level is signaled as E_{F0}. The splitting of the hole Fermi Level (E_{Fp}) and the electron Fermi Level (E_{Fn}) yields the output open-circuit voltage. Two extreme cases of (a) high and (b) low defect density are shown. Lower-lying levels are occupied in the case of low defect density, which produces the open-circuit voltage difference ΔVoc. Redrawn based on ref.[76]

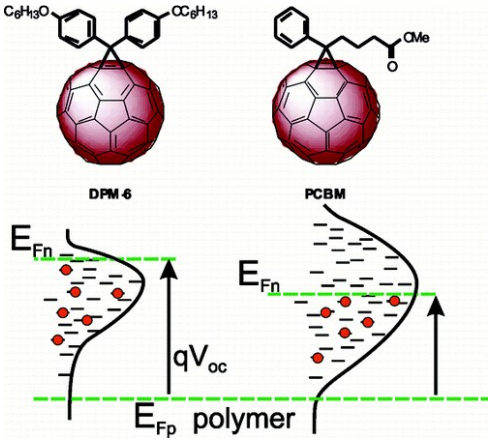

Figure 9b Correlation between the Open Circuit Voltage and the Energetics of Organic Bulk Heterojunction Solar Cells. Reprinted with permission from ref.[57] Copyright 2010 American Chemical Society.

However, as per the simple MIM model, which denotes that the V_{OC} is equal to the difference between the built-in voltage and the amount of band bending at each contact, is not quite accurate. In fact, V_{OC} varies with intensity, while band bending does not; likewise, band bending differs with the thickness of the active layer, while V_{OC}, in principle, does not.[26]

Measuring the variations in V_{OC} as a function of work function exemplifies the relationship amongst kinetics and relative quasi-Fermi levels.[77] During device operation, charges reorganize at the interface, when the work function of the contact is not aligned with the quasi-Fermi level of the active layer, thereby resulting in space-charge regions that modify the local electrochemical potential of the charge carriers and varies with respect to the distance from the contact.[77] The development of the space charge region at the interface modifies the

kinetics of charge carrier injection or extraction, relative to the rate of recombination intrinsic within the bulk heterojunction of the device.[77]

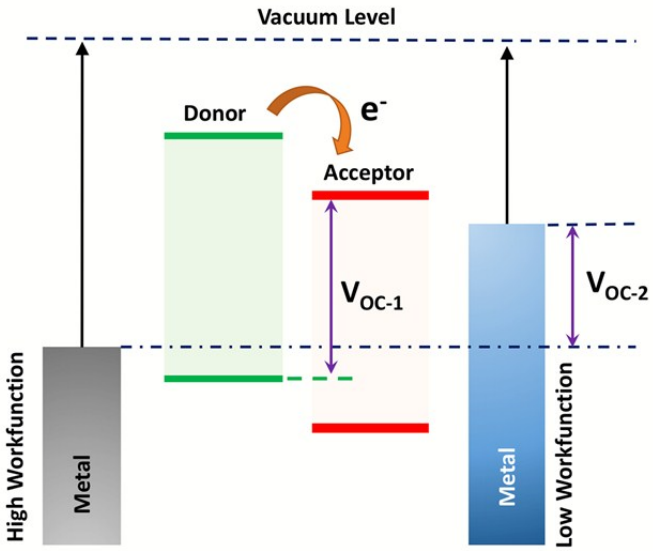

Figure 10. Open circuit voltage as governed by Donor-Acceptor interface (V_{oc-1}) when the contacts are ohmic. On the other hand, when the contacts are non-ohmic, Voc is determined by the work function difference of the electrode following Metal-Insulator-Metal (MIM) model (V_{oc-2}). Redrawn based on ref. [18].

Recently Andrea et al. validated the effect of the interface material layers and semiconductor energetic disorder on the V_{OC} in OSCs.[78] They investigated the physical dependence of V_{OC} on φ in P3HT: $PC_{60}BM$ devices and found that when the work function of the contacts is within the bandgap, the performance of the device depends intensely on even small variations of φ. Similarly, when work function approaches the energy levels of the semiconducting polymers i.e. near the LUMO and HOMO, device operation becomes the most effective and less sensitive to variations in φ as shown in Figure 11.

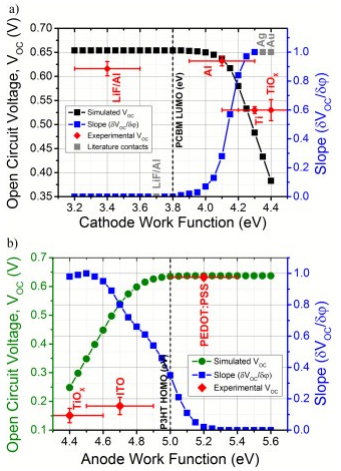

Figure 11. Simulated (black and green lines) and experimental V_{OC} (red line) as a function of cathode (a) and the anode (b) work functions and corresponding slope (blue line). Furthermore, in light grey the contact materials investigated from Mihailetchi et al. work[18] is considered - φ values of LiF/Al, Ag and Au reported in the article. Copyright with permission from ref.[78]

3.7.1 Relationship between V_{OC}, work function and DOS

In the previous section, we focussed on the relationship between V_{OC} and work function (φ). It is noteworthy to highlight the inter-relationship between the density of states (DOS) and work function (φ) on V_{OC} since the width and distribution of the DOS can be governed by chemical purity, morphology, etc. of the blend layer. The relationship between the simulated V_{OC} versus contact work function for various Gaussian density widths (σ) is shown in Figure 12(a).[78] It is observed that the anode and cathode work function vary symmetrically with respect to the middle of the blend band gap in the simulated trends. The V_{OC} depends linearly on $\Delta\varphi$ with minor effect on the Gaussian widths for $\Delta\varphi$ well near/closer to the middle of band gap ($0.05\ eV < \Delta\varphi < 0.25\ eV$) [see Figure 12(a)]. Furthermore, when the work function of anode and cathode are close to the center of band gap the V_{OC} is limited by the work function of the contacts, as predicted by MIM model in which the V_{OC} cannot outdo the built-in voltage (V_{BI}).[44, 78] On the other hand, when the work function difference becomes significant (i.e. $\Delta\varphi$ >0.25 eV), $\delta V_{OC}/\delta\varphi$ depends significantly on the width of the Gaussian DOS as shown in Figure 12(b). In addition, the final "saturated" value of V_{OC} varies intensely with the DOS (see Figure 12b). In fact, before V_{OC} saturation, $\delta V_{OC}/\delta\varphi$ almost approaches unity for highly ordered materials (where $\sigma \approx 50$ meV), since all the states are concentrated near to the median of the LUMO (fullerene) and HOMO (polymer) energy levels.[78]

In other words, upon photo-generation, the quasi Fermi levels split intensely (each closer to the median HOMO and LUMO energy levels) in the case of low disorder materials; thereby providing substantial amount of energy states for the photo-generated carriers to occupy. On the contrary for a highly disordered material ($\sigma \approx 150$ meV), the DOS tails extend deeply into the energy gap and the broadening of the HOMO and the LUMO energy levels is much greater.[78]

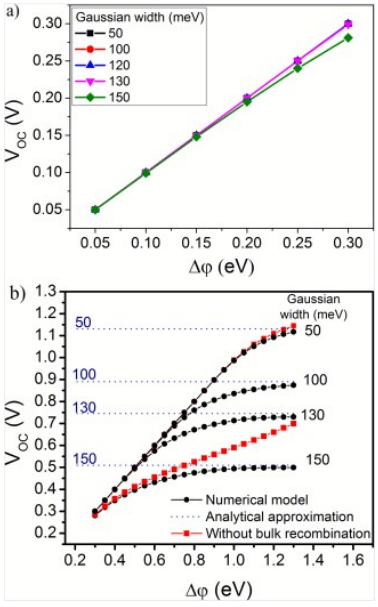

Figure 12. Simulated V_{OC} versus the anode-cathode work function difference for numerous values of the Gaussian DOS widths. In the simulation the work function are varied symmetrically with respect to the blend mid gap. a) Plot for low values of $\Delta\phi$ and b) plot for the entire variation of $\Delta\phi$. Here, the red lines are obtained without the inclusion of bulk recombination and only for the lowest and highest value of the Gaussian width. Copyright with permission from ref.[78]

3.7.2 Effect of Contact Selectivity on V_{OC}

Contact selectively is also one of the parameters that influence the V_{OC} in OSCs.[79, 80] In general, carriers that approach the contacts are also vulnerable to energy loss processes occurring at the interface, where charges may experience much greater carrier densities than in the bulk region because of spatially defined transport dynamics.[77] Moreover, at the active layer-contact interface, there is a continuous contest between extraction of free carriers and charge annihilation via recombination. Such competition manifests itself directly in the observed V_{OC} of the device. Therefore, any reduction in recombination at the interface will straightforwardly lead to increased V_{OC}, due to larger splitting of the quasi-Fermi levels.[77]

The term "selectivity" infers that there is a preferential collection of one charge and/or a concurrent decline in the rate of recombination with the other free charge carrier.[80-85] Mechanisms for realizing high carrier selective contacts may be obtained either by increasing the rate of preferred charge extraction or by reducing the rate of recombination.[77] Typically, the high charge selectivity is accomplished via the blocking of the undesired charge from reaching the respective contact by employing an energetic barrier while remaining energetically favourable for extraction of the preferred charge.[77]

In the case of electron blocking contacts, the existence of an energetic barrier to electron injection at the hole-collecting electrode reduces the dark reverse saturation current, eventually resulting in the rise in shunt resistance of the device. When a selective contact is used, it is also expected that a difference in the space charge region could be developed. As most of the blocking contacts are low carrier density oxides, it is quite possible that the intrinsic carrier density of the hole or electron blocking oxides to influence the width of the space charge region formed at the interfaces, and thus altering the rate of carrier extraction which in turn affects the V_{OC}.[77]

3.8 Charge transfer state (CT state)

Charge Transfer (CT) state complexes are interfacial electron–hole pairs located at the donor–acceptor (D/A) heterointerface as shown in Figure 13.[86-88] CT states are also known as polaron pairs,[87] exciplexes or charge transfer excitons.[86-88] The existence of charge transfer states has been demonstrated in numerous polymer/polymer and polymer/fullerene blends.[89, 90]

On the other hand, only a minor part/fraction of CT states would be filled under illumination owing to the low oscillator strength – one of the intrinsic properties of CT states. In a BHJ system, the acceptor singlet state and the CT state are the two kinds of energy states that are encountered by a photogenerated exciton when it approaches the D/A interface via diffusion. Here, CT states will not affect V_{OC} when the acceptor energy level of the singlet state is lower than that of the CT state. On the other hand, CT states will affect the V_{OC} when the excited exciton would populate the CT state if the CT state energy level were lower than the singlet state. In addition, the newly developed CT exciton will then either dissociate into polaron pairs or decay to the CT ground state.[91]

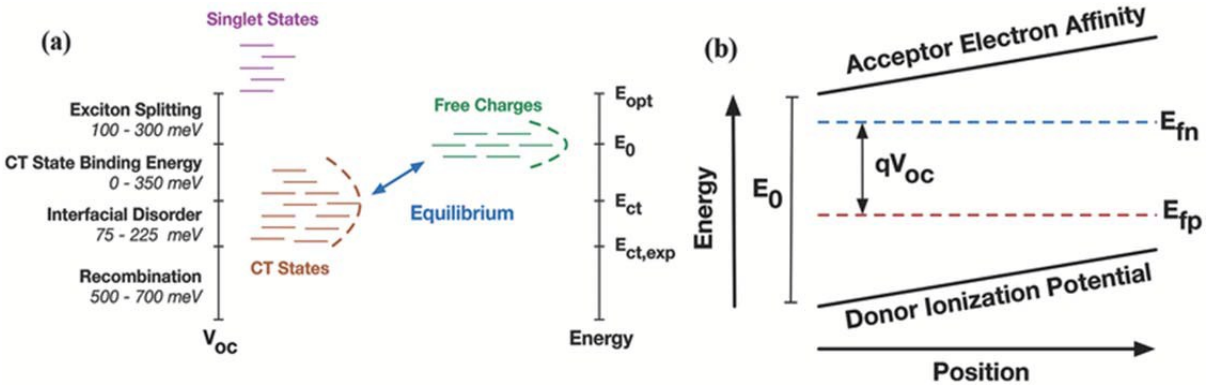

Figure 13 a) Depicts various sources of open-circuit voltage (Voc) losses from the optical gap in OSCs and various energy levels associated with it. b) Schematic band diagram of an organic solar cell at open-circuit showing the relationship between the quasi-Fermi levels for electrons (E_{fn}) and holes (E_{fp}), E_0, and the open-circuit voltage (V_{OC}). Reprinted with permission from ref.[99] Copyright 2015 WILEY-VCH Verlag GmbH & Co. KGaA.

A reciprocity relationship between photovoltaic quantum efficiency and electroluminescent emission (EQE_{EL}) based on the principle of Detailed Balance was proposed by Rau et al.,[92, 93] which is also applicable to organic donor–acceptor heterojunctions or BHJs. The following equation was derived based on that formulation to express V_{OC} for organic donor–acceptor junction cells:

$$V_{OC} = \frac{E_{CT}}{q} + \frac{k_B T}{q} ln\left(\frac{J_{SC} h^3 c^2}{f q 2\pi (E_{CT} - \lambda)}\right) + \frac{k_B T}{q} ln(EQE_{EL}) \quad (13)$$

Here E_{CT} is the free-energy difference between the CT excited state and the CT complex ground state, λ is the reorganization energy correlated with the CT absorption, c is the speed of light in a vacuum, f is a parameter proportional to the density of CT states and h is the Planck's constant. The last two terms in eqn.(13) illustrate the V_{OC} loss from non-radiative recombination and radiative recombination, respectively. Vandewal et al.[94] has deduced a relationship between J_0 and V_{OC} and their experimental results concur quite well with that of the model of CT states predicted in eqn 14. The dependence of V_{OC} on temperature T and illumination intensity P_0 was also successfully explained based on the model of CT states.

Vandewal et al.[23] also demonstrated the inter-relationship between charge-transfer absorption and emission and their influence on Voc using the detailed balance and quasi-equilibrium theory. It is shown that the electroluminescence (EL) and photovoltaic external quantum efficiency spectra (EQE_{PV}) in the low-energy, charge-transfer region are related to each other.[23] They also found that a weak-ground state interaction exists between the polymer and the fullerene; and deduced that the formation of such states significantly affects the Voc. Furthermore, it was also shown that at Voc, the recombination current exactly balances out the photogenerated current resulting in the emission of photons by the excited Charge-transfer complex (CTC), thereby suggesting that the Voc is determined by the CTC formation between the polymer and the fullerene.[23] It was also deduced that by increasing the EQE_{EL} by a factor of 10 would result in an increase of Voc of ~58 mV at room temperature via eliminating radiative recombinative pathways.[23] Similarly, Jenny Nelson and co-workers [41, 95] also employed electroluminescence (EL) and photoluminescence (PL) spectroscopy techniques to probe the energy of the interfacial states in a selection of high-performance polymers blended with a series of fullerenes. In their studies, they detected Fullerene triplet excitons in polymer: fullerene blends with high CT state energies and demonstrated that the formation of such triplet states occurs mainly when the offset energy

between the donor ionization potential and acceptor electron affinity is ~1.6 eV or greater.[41, 96] Faist et al. reported that the singlet activation in the EL occurs when the difference ΔE_{CS} between the energy of the CT emission, $E_{CT,EL}$, and the lowest component absorption onset, $E_{opt,min}$, is smaller than 0.35 eV.[95] (Refer Figure 14) By correlating the singlet excitation to the reduction in PL quenching and photocurrent generation, they observed that for the range $0 < \Delta E_{CS} < 0.35$ eV; a transition from pure CT emission to predominantly polymer or fullerene singlet emission occurs, in which the working devices exhibits strongly reduced photocurrent.[95] Based on this observation, an empirical limit for open circuit voltage for efficient polymer:fullerene solar cells is obtained as $V_{OC} \lesssim E_{opt,min}/e - (0.66 \pm 0.08)eV$ where $E_{opt,min} \equiv \min[E_{opt,donor}; E_{opt,acceptor}]$ is the minimum of the absorption onset of donor and acceptor.[95] Therefore raising the energy of the CT state via minimizing ΔE_{CS} without hindering efficient charge separation is consequently one of the major effective strategies for designing new donor and acceptor materials.[91, 95]

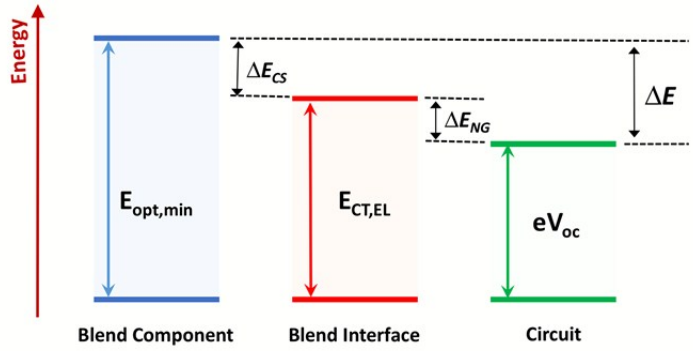

Figure 14. Schematic depicting the energetic losses in bulk heterojunction organic solar cells. ΔE_{CS} is the energetic loss between the smaller absorption onset of the two blend components ($E_{opt,min}$) and the peak of the CT state electroluminescence ($E_{CT,EL}$). ΔE_{NG} is the loss between ($E_{CT,EL}$) and the free energy of an electron at open circuit voltage (eV_{OC}); ΔE is the total energy loss. Redrawn based on ref.[95]

3.8.1 Relationship between V_{OC}, CT and DOS

As discussed earlier, in the Density of states (DOS) model, V_{OC} loss is attributed to tail states (within the band gap) in donor and acceptor material systems whereas in the case of charge transfer (CT) state model, V_{OC} loss is ascribed to charge carrier recombination at the donor–acceptor (D/A) interface by means of CT states. The dark saturation current is increased by the radiative and non-radiative recombination occurring at the CT states, correspondingly leading to the loss in V_{OC} according to eqn (5). CT states predominantly originates from the intermolecular interaction between the donor–acceptor materials at the (D/A) interface, therefore CT states resides only at the (D/A) heterojunction interface. On the other hand, tail states existing within the band gap of the donor and acceptor materials (affecting the distribution profile of the DOS), are associated with the properties of the material, which are intrinsically similar across the entire donor/acceptor film. Having discussed that, in both models the dominant recombination is bimolecular at open circuit conditions. Although, the CT state model explains the VOC loss convincingly, it has been debated till date that it is incapable to elucidate the super-bimolecular recombination noticed in some BHJ OSCs, which can be yet construed by the DOS model.[63, 97, 98]

3.8.2 Relationship between V_{OC}, Charge transfer (CT) states and free carriers

Burke et al. developed a relationship for the open-circuit voltage of OSCs based on the equilibrium between charge transfer (CT) states and free carriers.[99, 100] In order to deliver a driving force for the exciton splitting process to occur (during photo-generation at the D/A interface), donor (D) and acceptor (A) materials are characteristically selected to have electron affinities that differ by 0.1–0.3 eV, which also moderates qV_{oc} by the same amount.[101, 102] Therefore, V_{OC} is often referenced to the CT state energy rather than the optical gap as expressed in eqn. (14), since the voltage loss between optical absorption and CT state formation is believed to be an indispensable tradeoff to split the excitons efficiently.[46, 99, 101, 102] The relationship between V_{OC} and the average energy of the total CT states E_{ct} is expressed as[99]

$$qV_{OC} = E_{ct}^{exp} - kTlog\left(\frac{qfN_0L}{\tau_{ct}J_{sc}}\right) \quad (14)$$

where E_{ct} is the average energy of the total CT states in an organic solar cell, L is the thickness of the solar cell, J_{sc} is its short-circuit current, E_0 is the average difference between the electron affinity (EA) of the acceptor material and the ionization potential (IP) of the donor at the interface between the two, N_0 is the density of states (DOS) in the device, typically taken to be around 10^{21} cm^{-3} (1 nm^{-3}) for organic semiconductors and f is the volume fraction of the solar cell that is mixed or interfacial.[99] It is also demonstrated that each of the CT states recombines with an average lifetime $\tau_{ct} = 1/k_r$ and k_r is the (average) rate constant (at which CT states recombine).[99] Reducing the CT state binding energy and the interfacial energetic disorder could potentially raise V_{OC} by hundreds of mV without necessitating any modification to the CT state lifetime or degree of mixing.[99] The depiction of V_{OC} that materializes from this concept is one of a quantity that is limited mainly by the microscopic elements/characteristics of the interface between donor and acceptor molecules. By optimizing this interface, the researchers have the opportunity to substantially improve the PCE of OSCs through increase in V_{OC}.[99]

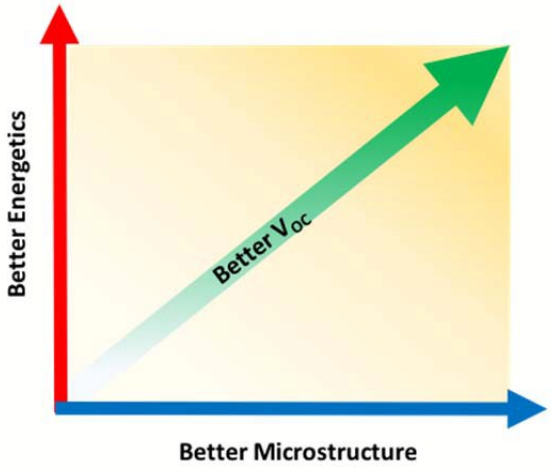

Figure 15: Schematic showing dependence of V_{OC} with better microstructure and energetics. Redrawn based on ref.[103].

3.9 Microstructure

Blend optimization with the focus on "microstructure" can be contemplated partially as a route for increasing carrier lifetimes adequately such that substantial recombination losses are moved towards higher carrier densities and therefore towards higher cell voltages. The term "microstructure" rather broadly refers to all aspects that could affect carrier dynamics and recombination rates excluding the charge-carrier densities and related mobilities.[103] The microstructural aspects may comprise the following: (a) domain size, (b) the existence of energetic barriers,(c) domain purity, (d) electric field gradients or dipoles at donor–acceptor interfaces, (e) the coulombic radius for the capture of charge carriers, and (f) the spatial distribution of intraband trap states.[103] Therefore, the influence of film microstructure on the energy levels of the materials, energetic disorder and charge carrier dynamics is essential for understanding and predicting the V_{OC} as shown in Figure 15.

Almost every high-efficiency OSCs developed so far were based on the approach of incorporating intermixed donor and acceptor molecules (blend) as the photon-harvesting active layer.[104-108] Implicit in this approach is the prerequisite that such blends must spontaneously change into an advantageous microstructure for carrier generation and collection, which can be achieved by appropriate deposition conditions or via post deposition treatments. Moreover, it was also demonstrated that the dependence of carrier lifetime on carrier density [$\tau(n)$] influences the total achievable V_{OC} in the device as shown in Figure 16(a & b).[103]

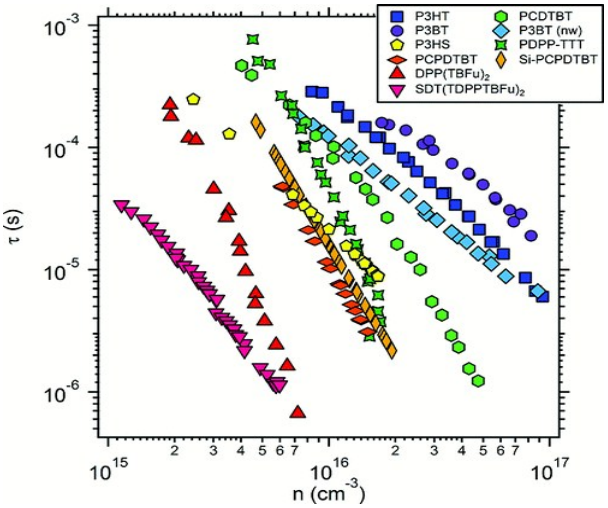

Figure 16a. Carrier lifetime versus average carrier density for various materials systems. Carrier lifetime is calculated from the small-perturbation lifetime obtained from TPV measurements using a power law approximation for τ(n). n is estimated from the total extractable charge with the contribution from the geometric (electrode) capacitance subtracted. Reprinted with permission from ref. [103] Copyright 2012 American Chemical Society.

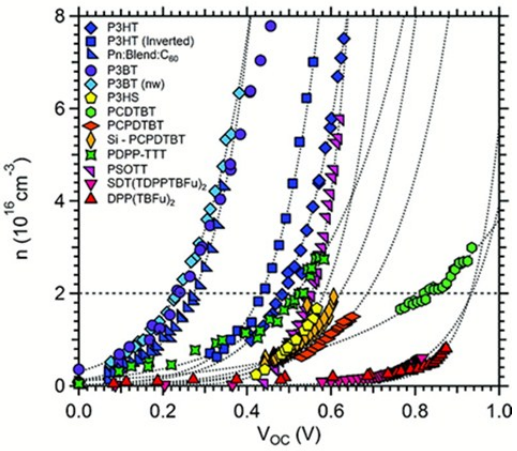

Figure 16b. V_{OC} measured as a function of carrier density for a number of material systems is depicted. Dashed gray lines are monoexponential characterizations of the data. Reprinted with permission from ref. [103] Copyright 2012 American Chemical Society.

Burke et al.[99] proposed that the density of states (DOS) of the light absorbing active layer, as dictated by the extent of energetic disorder, the molecular orbital levels, and crystallinity, is not substantially correlated with carrier lifetime (τ). Moreover, the carrier lifetime would significantly depend on the physical interaction between those states and consequently on the detailed microstructure of the blend which implicitly denotes the carrier mobility of the blend.[103] They also demonstrated that while some intermixing of blend components is obviously essential for proficient exciton quenching, excess of it can result in significant loss of achievable voltage.[99, 103] It was found that upto 200–300 mV is lost between highly phase-separated systems with slow recombination, such as P3HT and P3BT, and highly intermixed systems qualified with fast recombination, such as DPP(TBFu)$_2$ and PCPDTBT (see Figure 16(a & b)).[103] Therefore, for achieving high V_{OC} it is necessary not only to tailor the energy levels of the blend components/materials but also to increase the carrier lifetimes within the active layer via tuning the blend microstructure.

3.10 Morphology

Relating morphological characteristics to the open-circuit voltage of OSCs is an open debate till date.[109] Even though the BHJ-OPV improves J_{SC}, reports have revealed that morphology does not seem to have considerable effect on V_{OC}.[110-112] Adding to this argument, Alam et al.[113] provided an explicit analytical proof demonstrating that any effort to radically increase V_{OC} by tailoring bulk heterojunction morphology is futile, because any increase in J_{SC} due to larger interface area is compensated by corresponding increase in recombination current. Thereby, the upper limit of Voc_{BHJ} cannot exceed that of the corresponding planar heterojunction devices, i.e., $Voc_{BHJ} \leq Voc_{PHJ}$. Having said that, a distinct morphological feature i.e. the ratio between the donor volume fraction and the specific interfacial area (γ_δ/a_v) is found to play a significant role in determining the V_{OC} of OSCs.[109] On the other hand, morphological characteristics of the donor/acceptor blend, such as the connectivity of percolation pathways, do not have substantial impact on the V_{OC}. Zhang et al. [109] related V_{OC} with the magnitude of the average exciton flux (j_{ex}^{avg}) which is expressed as

$$V_{OC} = \frac{E_g^{eff}}{e} + \frac{k_B T}{e} ln\left[\frac{P j_{ex}^{avg}}{h(1-P)k_r N_{CV}^2}\right] \quad (15)$$

Where E_g^{eff} is the effective band gap, N_{cv} is the effective density of states at both positive and negative contacts, T is the temperature, P is the dissociation probability of the interfacial charge-transfer state, k_r is the Langevin bimolecular recombination constant, j_{ex}^{avg} is the magnitude of the average exciton flux towards D/A interfaces, h is the interfacial lengths scale, e is the elementary charge and k_B is the Boltzmann constant.[109]

The relation, Eq. (15) is equivalent to the V_{OC} expression proposed by Koster et al.[62] for BHJ OSCs as well as the one reported by Giebink et al. for PHJ OSCs,[114] except that Eq. (15) incorporates the added influence of the donor acceptor (D/A) morphology on V_{OC} and characteristically resolve morphological features of the order of the phase-separation length scale (~10 nm).[109] Moreover, morphological disorders existing on the molecular and atomistic scales, because of the factors such as variations in conjugation length, impurities, rotations and

kinking of polymer chains, etc. could alter material properties like E_g^{eff} and k_r considerably and thus may influence V_{OC}.[103] The expression (eqn. 15) also elucidates that the key influence of morphology on the V_{OC} can be attributed to a single morphological parameter: the ratio between the donor volume fraction and the specific interfacial area, (γ_δ/a_v).[109] The open-circuit voltage of OSCs rises with increasing γ_δ and decreases with increasing a_v. It simply implies that by attaining well-ordered D/A morphologies does not result in significant improvements of the V_{OC}.[109]

3.11 Donor-Acceptor Interface Area

Vandewal et al.[115] recently demonstrated that the charge carrier lifetime in small molecule: C_{60} photovoltaic devices are augmented by decreasing the physical interface area available for recombination, thereby improving the V_{OC}. They also observed when the donor contents below 10%, V_{OC} improved logarithmically corresponding the interface area while the energy of the interfacial charge-transfer state E_{CT} remains constant as shown in Figure 17.

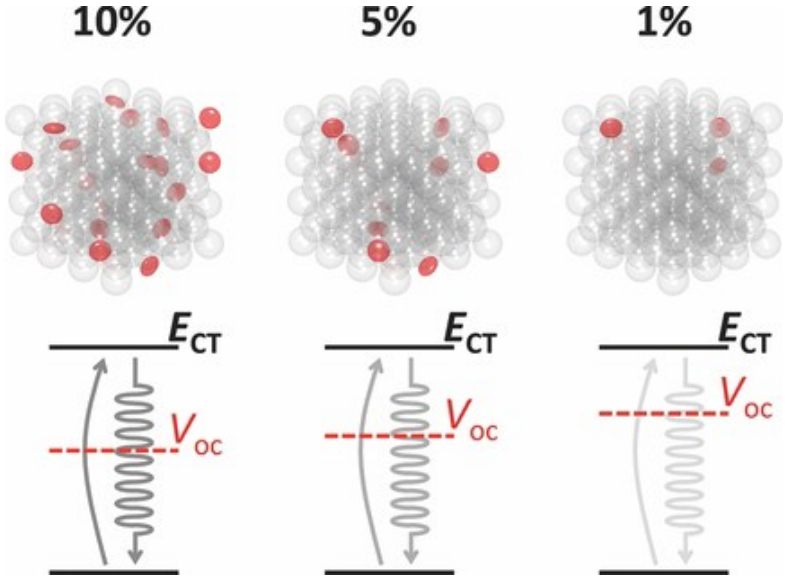

Figure 17. Effect of Donor-Acceptor interfacial area on V_{OC}. The V_{OC} varies with percentage reduction of interfacial area without any significant effect on E_{CT}. Reprinted with permission from ref.[115] Copyright 2014 WILEY-VCH Verlag GmbH & Co. KGaA.

Vandewal et al. determined E_{CT} by employing sensitive measurement techniques such electroluminescence (EL) emission spectra in their experiment. They found that certain photon energies below the optical gap of both donor and acceptor material was analysed, to determine the weak absorption and emission bands corresponding to the direct CT state excitation and recombination.[94, 116] They correlated the amplitude of the low energy CT absorption band (in the EQE spectra) with the amount of ground state D-A complexes and found that it is proportional to the interfacial area.

It was found that by changing the donor concentration and consequently the interfacial area in the low donor regime, E_{CT} remains constant. However, V_{OC} can be increased substantially say ~ (80–150 meV), solely by a 10-

fold reduction in interfacial area, under the condition that proper Ohmic contacts are employed. Their findings provide the foundation for a new design paradigm for organic solar cells with increased V_{OC}.[115]

4. Future Strategies and Conclusion

Before discussing the possible strategies to improve V_{OC}, it is worthy to mention that the degree of influence of the various factors affecting V_{OC} is not equal. From future development point of view, factors such as energetic disorder, CT states, microstructure, D/A interface area etc. play a predominant role in determining the V_{OC} and hold a larger ground for research and improvement. Considering this discussion, some of the probable ways to improve V_{OC} are listed below,

1. One of the key prospects for improving the V_{OC} is to reduce the density of trap states via proper control of the phase-separated morphology and by altering the interfacial composition of the donor acceptor materials. Such approach of decreasing the interfacial trap density would also facilitate the fabrication of thick photoactive layer, which in turn would increase the short circuit current without compromising the fill factor.
2. Decreasing the conformational disorder arising at the interface, by engineering the donor and acceptor materials to exhibit preferred orientations is another promising way to improve the V_{OC}.[117] For instance, a small reduction in interfacial disorder contributes about 100 mV to the open-circuit voltage of the regio-regular blend (P3HT:PCBM).[118]
3. Improving the contact work function difference by proper selection of materials (in order to reach the saturation regime of $\delta V_{OC}/\delta\varphi$ for both cathode and anode) along with reducing the width of the Gaussian DOS is one of the promising paths for increasing the V_{OC}. This can be accomplished via careful synthesis and controlled deposition of the blend.
4. Designing donor molecules with greater degree of delocalized wave function reduces the binding energy of the CT states, which directly improves the V_{OC}. Furthermore, improving the dielectric constant of the active layer is also an efficient way for increasing the V_{OC}. A slight increase in dielectric constant ~5 significantly lowers/eliminates the CT state binding energy by making the CT states more delocalized.[119]
5. Increasing the lifetime of the CT states is another way to improve the V_{OC}. The dynamic nature of the donor/acceptor interface is speculated to play a significant role in permitting CT states to attain configurations favourable for fast non-radiative recombination. It has been demonstrated that the lifetime of the CT states are governed by the non-radiative transitions with EQE typically lower than 10^{-6}.[94] Considering this scenario, securing the donor/acceptor conformation could be a crucial and important way to increase the radiative quantum efficiency and hence the V_{OC}.
6. Open circuit voltage V_{OC}, could also be tuned independently of the interfacial energetics, and is contingent on the interfacial area accessible for charge carrier recombination. Intuitively, it implies that an optimal interfacial area at a donor/acceptor heterojunction should be adequately large enough to ensure efficient exciton dissociation, simultaneously exhibiting long charge carrier lifetime - favourable for achieving high V_{OC}. Therefore, designing of organic semiconductor materials with larger exciton diffusion lengths

would enable a reduced optimum interfacial area and thereby producing a smaller E_{CT}-qV_{oc} difference, which could ultimately result in higher PCEs.

In conclusion, the open circuit voltage (V_{OC}) plays a predominant role in determining the power conversion efficiency (PCE). V_{OC} depends on a variety of parameters as discussed in this review including elaborations on specifics to improve the V_{OC}. Even though all of the influencing parameters are significant, few parameters among them such as density of states (DOS) distribution or energetic disorder, Charge Transfer (CT) states, microstructure and donor/acceptor (D/A) interface area etc. endures more weightage from a vantage point focussed on future development. In spite of exhaustive discussions, it cannot be pointed out that one particular universal model serves as the panacea for resolving the V_{OC} issues and to drive them towards greater frontiers. As novel materials are invented each day and the sensitivity and sophistication of characterization techniques have evolved, the field of V_{OC} research would remain a subject of on-going research at-least till near future.

5. References

1. A. Facchetti, *Chemistry of Materials*, 2011, **23**, 733-758.
2. U. Zhokhavets, T. Erb, G. Gobsch, M. Al-Ibrahim and O. Ambacher, *Chemical Physics Letters*, 2006, **418**, 347-350.
3. G. Yu, J. Gao, J. C. Hummelen, F. Wudl and A. J. Heeger, *Science*, 1995, **270**, 1789-1791.
4. C. W. Tang, *Applied Physics Letters*, 1986, **48**, 183-185.
5. H. Gmbh, T. U. Dresden and V. Whereas, *Heliatek press release*, 2013, 1-3.
6. E. Bundgaard and F. C. Krebs, *Solar Energy Materials and Solar Cells*, 2007, **91**, 954-985.
7. Y. Liang and L. Yu, *Polymer Reviews*, 2010, **50**, 454-473.
8. J. Peet, J. Y. Kim, N. E. Coates, W. L. Ma, D. Moses, A. J. Heeger and G. C. Bazan, *Nat Mater*, 2007, **6**, 497-500.
9. S. B. Darling and F. You, *RSC Advances*, 2013, **3**, 17633-17648.
10. M. D. Perez, C. Borek, S. R. Forrest and M. E. Thompson, *Journal of the American Chemical Society*, 2009, **131**, 9281-9286.
11. W. Shockley and H. J. Queisser, *Journal of Applied Physics*, 1961, **32**, 510-519.
12. R. T. Ross, *The Journal of Chemical Physics*, 1967, **46**, 4590-4593.
13. C. J. Brabec, A. Cravino, D. Meissner, N. S. Sariciftci, T. Fromherz, M. T. Rispens, L. Sanchez and J. C. Hummelen, *Advanced Functional Materials*, 2001, **11**, 374-380.
14. M. C. Scharber, D. Mühlbacher, M. Koppe, P. Denk, C. Waldauf, A. J. Heeger and C. J. Brabec, *Advanced Materials*, 2006, **18**, 789-794.
15. D. Veldman, S. C. J. Meskers and R. A. J. Janssen, *Advanced Functional Materials*, 2009, **19**, 1939-1948.
16. K. Vandewal, A. Gadisa, W. D. Oosterbaan, S. Bertho, F. Banishoeib, I. Van Severen, L. Lutsen, T. J. Cleij, D. Vanderzande and J. V. Manca, *Advanced Functional Materials*, 2008, **18**, 2064-2070.
17. T. Kietzke, D. A. M. Egbe, H.-H. Hörhold and D. Neher, *Macromolecules*, 2006, **39**, 4018-4022.
18. V. D. Mihailetchi, P. W. M. Blom, J. C. Hummelen and M. T. Rispens, *Journal of Applied Physics*, 2003, **94**, 6849-6854.
19. V. Lemaur, M. Steel, D. Beljonne, J.-L. Brédas and J. Cornil, *Journal of the American Chemical Society*, 2005, **127**, 6077-6086.
20. G. Li, R. Zhu and Y. Yang, *Nat Photon*, 2012, **6**, 153-161.
21. H. Bässler, *physica status solidi (b)*, 1993, **175**, 15-56.
22. G. Dennler, M. C. Scharber and C. J. Brabec, *Advanced Materials*, 2009, **21**, 1323-1338.
23. K. Vandewal, K. Tvingstedt, A. Gadisa, O. Inganas and J. V. Manca, *Nat Mater*, 2009, **8**, 904-909.
24. B. Qi and J. Wang, *Journal of Materials Chemistry*, 2012, **22**, 24315-24325.
25. I. Lange, J. Kniepert, P. Pingel, I. Dumsch, S. Allard, S. Janietz, U. Scherf and D. Neher, *The Journal of Physical Chemistry Letters*, 2013, **4**, 3865-3871.
26. J. C. Blakesley and D. Neher, *Physical Review B*, 2011, **84**, 075210.
27. P. Würfel and U. Würfel, *Physics of Solar Cells: From Basic Principles to Advanced Concepts*, Wiley, 2009.
28. W. J. Potscavage, S. Yoo and B. Kippelen, *Applied Physics Letters*, 2008, **93**, 193308.
29. W. J. Potscavage, A. Sharma and B. Kippelen, *Accounts of Chemical Research*, 2009, **42**, 1758-1767.
30. P. Schilinsky, C. Waldauf and C. J. Brabec, *Applied Physics Letters*, 2002, **81**, 3885-3887.
31. I. Riedel, J. Parisi, V. Dyakonov, L. Lutsen, D. Vanderzande and J. C. Hummelen, *Advanced Functional Materials*, 2004, **14**, 38-44.
32. B. P. Rand, D. P. Burk and S. R. Forrest, *Physical Review B*, 2007, **75**, 115327.
33. P. Peumans, A. Yakimov and S. R. Forrest, *Journal of Applied Physics*, 2003, **93**, 3693-3723.
34. R. Signerski, *Journal of Non-Crystalline Solids*, 2008, **354**, 4465-4468.
35. G. Smestad and H. Ries, *Solar Energy Materials and Solar Cells*, 1992, **25**, 51-71.
36. T. Markvart, *Applied Physics Letters*, 2007, **91**, 064102.

37. T. Markvart, *physica status solidi (a)*, 2008, **205**, 2752-2756.
38. O. D. Miller, E. Yablonovitch and S. R. Kurtz, *Photovoltaics, IEEE Journal of*, 2012, **2**, 303-311.
39. J. Nelson, J. Kirkpatrick and P. Ravirajan, *Physical Review B*, 2004, **69**, 035337.
40. A. Maurano, R. Hamilton, C. G. Shuttle, A. M. Ballantyne, J. Nelson, B. O'Regan, W. Zhang, I. McCulloch, H. Azimi, M. Morana, C. J. Brabec and J. R. Durrant, *Advanced Materials*, 2010, **22**, 4987-4992.
41. C. Dyer-Smith, L. X. Reynolds, A. Bruno, D. D. C. Bradley, S. A. Haque and J. Nelson, *Advanced Functional Materials*, 2010, **20**, 2701-2708.
42. S. R. Cowan, A. Roy and A. J. Heeger, *Physical Review B*, 2010, **82**, 245207.
43. C. G. Shuttle, A. Maurano, R. Hamilton, B. O'Regan, J. C. de Mello and J. R. Durrant, *Applied Physics Letters*, 2008, **93**, 183501.
44. P. W. M. Blom, V. D. Mihailetchi, L. J. A. Koster and D. E. Markov, *Advanced Materials*, 2007, **19**, 1551-1566.
45. R. A. Street, M. Schoendorf, A. Roy and J. H. Lee, *Physical Review B*, 2010, **81**, 205307.
46. K. R. Graham, P. Erwin, D. Nordlund, K. Vandewal, R. Li, G. O. Ngongang Ndjawa, E. T. Hoke, A. Salleo, M. E. Thompson, M. D. McGehee and A. Amassian, *Advanced Materials*, 2013, **25**, 6076-6082.
47. P. M. Beaujuge and J. M. J. Fréchet, *Journal of the American Chemical Society*, 2011, **133**, 20009-20029.
48. E. A. Katz, D. Faiman, S. M. Tuladhar, J. M. Kroon, M. M. Wienk, T. Fromherz, F. Padinger, C. J. Brabec and N. S. Sariciftci, *Journal of Applied Physics*, 2001, **90**, 5343-5350.
49. D. Chirvase, Z. Chiguvare, M. Knipper, J. Parisi, V. Dyakonov and J. C. Hummelen, *Journal of Applied Physics*, 2003, **93**, 3376-3383.
50. M. Kemerink, J. M. Kramer, H. H. P. Gommans and R. A. J. Janssen, *Applied Physics Letters*, 2006, **88**, 192108.
51. L. J. A. Koster, E. C. P. Smits, V. D. Mihailetchi and P. W. M. Blom, *Physical Review B*, 2005, **72**, 085205.
52. F. C. Krebs, S. A. Gevorgyan, B. Gholamkhass, S. Holdcroft, C. Schlenker, M. E. Thompson, B. C. Thompson, D. Olson, D. S. Ginley, S. E. Shaheen, H. N. Alshareef, J. W. Murphy, W. J. Youngblood, N. C. Heston, J. R. Reynolds, S. Jia, D. Laird, S. M. Tuladhar, J. G. A. Dane, P. Atienzar, J. Nelson, J. M. Kroon, M. M. Wienk, R. A. J. Janssen, K. Tvingstedt, F. Zhang, M. Andersson, O. Inganäs, M. Lira-Cantu, R. de Bettignies, S. Guillerez, T. Aernouts, D. Cheyns, L. Lutsen, B. Zimmermann, U. Würfel, M. Niggemann, H.-F. Schleiermacher, P. Liska, M. Grätzel, P. Lianos, E. A. Katz, W. Lohwasser and B. Jannon, *Solar Energy Materials and Solar Cells*, 2009, **93**, 1968-1977.
53. F. Gao, W. Tress, J. Wang and O. Inganäs, *Physical Review Letters*, 2015, **114**, 128701.
54. N. K. Elumalai, C. Vijila, R. Jose, K. Zhi Ming, A. Saha and S. Ramakrishna, *Physical Chemistry Chemical Physics*, 2013, **15**, 19057-19064.
55. N. K. Elumalai, A. Saha, C. Vijila, R. Jose, Z. Jie and S. Ramakrishna, *Physical Chemistry Chemical Physics*, 2013, **15**, 6831-6841.
56. V. D. Mihailetchi, J. K. J. van Duren, P. W. M. Blom, J. C. Hummelen, R. A. J. Janssen, J. M. Kroon, M. T. Rispens, W. J. H. Verhees and M. M. Wienk, *Advanced Functional Materials*, 2003, **13**, 43-46.
57. G. Garcia-Belmonte, P. P. Boix, J. Bisquert, M. Lenes, H. J. Bolink, A. La Rosa, S. Filippone and N. Martín, *The Journal of Physical Chemistry Letters*, 2010, **1**, 2566-2571.
58. A. K. Thakur, G. Wantz, G. Garcia-Belmonte, J. Bisquert and L. Hirsch, *Solar Energy Materials and Solar Cells*, 2011, **95**, 2131-2135.
59. G. Garcia-Belmonte, *Solar Energy Materials and Solar Cells*, 2010, **94**, 2166-2169.
60. G. Garcia-Belmonte and J. Bisquert, *Applied Physics Letters*, 2010, **96**, 113301.
61. J. Bisquert, D. Cahen, G. Hodes, S. Rühle and A. Zaban, *The Journal of Physical Chemistry B*, 2004, **108**, 8106-8118.
62. L. J. A. Koster, V. D. Mihailetchi, R. Ramaker and P. W. M. Blom, *Applied Physics Letters*, 2005, **86**, 123509.

63. G. Garcia-Belmonte, P. P. Boix, J. Bisquert, M. Sessolo and H. J. Bolink, *Solar Energy Materials and Solar Cells*, 2010, **94**, 366-375.
64. T. Kirchartz, K. Taretto and U. Rau, *The Journal of Physical Chemistry C*, 2009, **113**, 17958-17966.
65. J. Bisquert, G. Garcia-Belmonte and J. García-Cañadas, *The Journal of Chemical Physics*, 2004, **120**, 6726-6733.
66. L. G. Kaake, P. F. Barbara and X. Y. Zhu, *The Journal of Physical Chemistry Letters*, 2010, **1**, 628-635.
67. T. Sueyoshi, H. Fukagawa, M. Ono, S. Kera and N. Ueno, *Applied Physics Letters*, 2009, **95**, 183303.
68. O. Tal, Y. Rosenwaks, Y. Preezant, N. Tessler, C. K. Chan and A. Kahn, *Physical Review Letters*, 2005, **95**, 256405.
69. I. N. Hulea, H. B. Brom, A. J. Houtepen, D. Vanmaekelbergh, J. J. Kelly and E. A. Meulenkamp, *Physical Review Letters*, 2004, **93**, 166601.
70. K. Celebi, P. J. Jadhav, K. M. Milaninia, M. Bora and M. A. Baldo, *Applied Physics Letters*, 2008, **93**, 083308.
71. S. L. M. van Mensfoort and R. Coehoorn, *Physical Review B*, 2008, **78**, 085207.
72. C. Tanase, E. J. Meijer, P. W. M. Blom and D. M. de Leeuw, *Physical Review Letters*, 2003, **91**, 216601.
73. J. C. Blakesley, H. S. Clubb and N. C. Greenham, *Physical Review B*, 2010, **81**, 045210.
74. I. Lange, J. C. Blakesley, J. Frisch, A. Vollmer, N. Koch and D. Neher, *Physical Review Letters*, 2011, **106**, 216402.
75. V. I. Arkhipov, E. V. Emelianova, Y. H. Tak and H. Bässler, *Journal of Applied Physics*, 1998, **84**, 848-856.
76. T. S. Ripolles, A. Guerrero and G. Garcia-Belmonte, *Applied Physics Letters*, 2013, **103**, 243306.
77. E. L. Ratcliff, A. Garcia, S. A. Paniagua, S. R. Cowan, A. J. Giordano, D. S. Ginley, S. R. Marder, J. J. Berry and D. C. Olson, *Advanced Energy Materials*, 2013, **3**, 647-656.
78. A. Zampetti, A. H. Fallahpour, M. Dianetti, L. Salamandra, F. Santoni, A. Gagliardi, M. Auf der Maur, F. Brunetti, A. Reale, T. M. Brown and A. Di Carlo, *Journal of Polymer Science Part B: Polymer Physics*, 2015, **53**, 690-699.
79. N. Elumalai, C. Vijila, R. Jose, A. Uddin and S. Ramakrishna, *Mater Renew Sustain Energy*, 2015, **4**, 1-25.
80. R. Steim, F. R. Kogler and C. J. Brabec, *Journal of Materials Chemistry*, 2010, **20**, 2499-2512.
81. E. L. Ratcliff, B. Zacher and N. R. Armstrong, *The Journal of Physical Chemistry Letters*, 2011, **2**, 1337-1350.
82. Y. Sun, C. J. Takacs, S. R. Cowan, J. H. Seo, X. Gong, A. Roy and A. J. Heeger, *Advanced Materials*, 2011, **23**, 2226-2230.
83. Y. Sun, J. H. Seo, C. J. Takacs, J. Seifter and A. J. Heeger, *Advanced Materials*, 2011, **23**, 1679-1683.
84. E. L. Ratcliff, J. Meyer, K. X. Steirer, A. Garcia, J. J. Berry, D. S. Ginley, D. C. Olson, A. Kahn and N. R. Armstrong, *Chemistry of Materials*, 2011, **23**, 4988-5000.
85. K. X. Steirer, J. P. Chesin, N. E. Widjonarko, J. J. Berry, A. Miedaner, D. S. Ginley and D. C. Olson, *Organic Electronics*, 2010, **11**, 1414-1418.
86. D. Veldman, Ö. İpek, S. C. J. Meskers, J. Sweelssen, M. M. Koetse, S. C. Veenstra, J. M. Kroon, S. S. v. Bavel, J. Loos and R. A. J. Janssen, *Journal of the American Chemical Society*, 2008, **130**, 7721-7735.
87. V. Dyakonov and E. Frankevich, *Chemical Physics*, 1998, **227**, 203-217.
88. A. C. Morteani, P. Sreearunothai, L. M. Herz, R. H. Friend and C. Silva, *Physical Review Letters*, 2004, **92**, 247402.
89. H. Ohkita, S. Cook, Y. Astuti, W. Duffy, S. Tierney, W. Zhang, M. Heeney, I. McCulloch, J. Nelson, D. D. C. Bradley and J. R. Durrant, *Journal of the American Chemical Society*, 2008, **130**, 3030-3042.

90. Y. Zhou, K. Tvingstedt, F. Zhang, C. Du, W.-X. Ni, M. R. Andersson and O. Inganäs, *Advanced Functional Materials*, 2009, **19**, 3293-3299.
91. C. Deibel, T. Strobel and V. Dyakonov, *Advanced Materials*, 2010, **22**, 4097-4111.
92. T. Kirchartz and U. Rau, *physica status solidi (a)*, 2008, **205**, 2737-2751.
93. U. Rau, *Physical Review B*, 2007, **76**, 085303.
94. K. Vandewal, K. Tvingstedt, A. Gadisa, O. Inganäs and J. V. Manca, *Physical Review B*, 2010, **81**, 125204.
95. M. A. Faist, T. Kirchartz, W. Gong, R. S. Ashraf, I. McCulloch, J. C. de Mello, N. J. Ekins-Daukes, D. D. Bradley and J. Nelson, *J Am Chem Soc*, 2012, **134**, 685-692.
96. J. J. Benson-Smith, H. Ohkita, S. Cook, J. R. Durrant, D. D. C. Bradley and J. Nelson, *Dalton Transactions*, 2009, DOI: 10.1039/B910675H, 10000-10005.
97. C. G. Shuttle, B. O'Regan, A. M. Ballantyne, J. Nelson, D. D. C. Bradley, J. de Mello and J. R. Durrant, *Applied Physics Letters*, 2008, **92**, 093311.
98. G. Juška, K. Genevičius, N. Nekrašas, G. Sliaužys and G. Dennler, *Applied Physics Letters*, 2008, **93**, 143303.
99. T. M. Burke, S. Sweetnam, K. Vandewal and M. D. McGehee, *Advanced Energy Materials*, 2015, **5**, n/a-n/a.
100. B. Kippelen and J.-L. Bredas, *Energy & Environmental Science*, 2009, **2**, 251-261.
101. E. T. Hoke, K. Vandewal, J. A. Bartelt, W. R. Mateker, J. D. Douglas, R. Noriega, K. R. Graham, J. M. J. Fréchet, A. Salleo and M. D. McGehee, *Advanced Energy Materials*, 2013, **3**, 220-230.
102. T. M. Clarke and J. R. Durrant, *Chemical Reviews*, 2010, **110**, 6736-6767.
103. D. Credgington and J. R. Durrant, *The Journal of Physical Chemistry Letters*, 2012, **3**, 1465-1478.
104. Y. Liang, Z. Xu, J. Xia, S.-T. Tsai, Y. Wu, G. Li, C. Ray and L. Yu, *Advanced Materials*, 2010, **22**, E135-E138.
105. S. Dayal, M. O. Reese, A. J. Ferguson, D. S. Ginley, G. Rumbles and N. Kopidakis, *Advanced Functional Materials*, 2010, **20**, 2629-2635.
106. H. Bronstein, Z. Chen, R. S. Ashraf, W. Zhang, J. Du, J. R. Durrant, P. Shakya Tuladhar, K. Song, S. E. Watkins, Y. Geerts, M. M. Wienk, R. A. J. Janssen, T. Anthopoulos, H. Sirringhaus, M. Heeney and I. McCulloch, *Journal of the American Chemical Society*, 2011, **133**, 3272-3275.
107. B. Walker, C. Kim and T.-Q. Nguyen, *Chemistry of Materials*, 2011, **23**, 470-482.
108. M. Riede, C. Uhrich, J. Widmer, R. Timmreck, D. Wynands, G. Schwartz, W.-M. Gnehr, D. Hildebrandt, A. Weiss, J. Hwang, S. Sundarraj, P. Erk, M. Pfeiffer and K. Leo, *Advanced Functional Materials*, 2011, **21**, 3019-3028.
109. Z. Teng, B. Erik and L. Joachim, *Applied Physics Express*, 2015, **8**, 024301.
110. J. A. Barker, C. M. Ramsdale and N. C. Greenham, *Physical Review B*, 2003, **67**, 075205.
111. B. Ray and M. A. Alam, *Solar Energy Materials and Solar Cells*, 2012, **99**, 204-212.
112. G. A. Buxton and N. Clarke, *Physical Review B*, 2006, **74**, 085207.
113. B. Ray, P. R. Nair and M. A. Alam, 2010.
114. N. C. Giebink, G. P. Wiederrecht, M. R. Wasielewski and S. R. Forrest, *Physical Review B*, 2010, **82**, 155305.
115. K. Vandewal, J. Widmer, T. Heumueller, C. J. Brabec, M. D. McGehee, K. Leo, M. Riede and A. Salleo, *Advanced Materials*, 2014, **26**, 3839-3843.
116. K. Tvingstedt, K. Vandewal, A. Gadisa, F. Zhang, J. Manca and O. Inganäs, *Journal of the American Chemical Society*, 2009, **131**, 11819-11824.
117. K. R. Graham, C. Cabanetos, J. P. Jahnke, M. N. Idso, A. El Labban, G. O. Ngongang Ndjawa, T. Heumueller, K. Vandewal, A. Salleo, B. F. Chmelka, A. Amassian, P. M. Beaujuge and M. D. McGehee, *Journal of the American Chemical Society*, 2014, **136**, 9608-9618.
118. W. C. Tsoi, S. J. Spencer, L. Yang, A. M. Ballantyne, P. G. Nicholson, A. Turnbull, A. G. Shard, C. E. Murphy, D. D. C. Bradley, J. Nelson and J.-S. Kim, *Macromolecules*, 2011, **44**, 2944-2952.

119. S. Chen, S.-W. Tsang, T.-H. Lai, J. R. Reynolds and F. So, *Advanced Materials*, 2014, **26**, 6125-6131.

Broader context

Sustainable renewable energy technologies form the major component of the future global energy strategy to solve the foreseeable world's energy crisis. Harnessing the energy from the sun is certainly one of the most pragmatic pathways to cater the global energy needs. Organic solar cells (OSCs) represent a transformative solar technology with prodigious potential for exceptionally high-throughput manufacturing at very low cost, and are made from non-toxic, earth-abundant materials with low energy inputs. Organic photovoltaics are particularly attractive because of their mechanical flexibility and ease of processing, which makes it an ideal candidate to serve as power sources for various commercial applications. Despite the potential of OPVs for large-scale solar deployment, their performance efficiencies are not high enough to consent direct competition against mature photovoltaic technologies. One of the most important parameter that determines the efficiency of OSCs is the open-circuit voltage (V_{OC}), which represents the maximum voltage a solar cell can provide to an external circuit. This review elaborates the origin, fundamental governing mechanisms and associated energetic loss processes that influence the V_{OC} of the OSCs – providing a comprehensive understanding of Voc and could help researchers to develop better materials and devices.

TOC /Graphical abstract

Factors and governing mechanisms influencing the open circuit voltage – a key determinant for improving the device performance efficiency